Importance of Photochemical Reactions for the Hydroxyl Radical Concentration and Methane Lifetime

- A Counterfactual Investigation

Dina Stabell

Thesis submitted for the degree of
Master of science in Meteorology and Oceanography
60 Credits

Department of Geosciences
Faculty of mathematics and natural sciences

UNIVERSITY OF OSLO

August 14, 2020

Importance of Photochemical Reactions for the Hydroxyl Radical Concentration and Methane Lifetime
- A Counterfactual Investigation

This work is published digitally through DUO – Digitale Utgivelser ved UiO
`http://www.duo.uio.no/`

Printed: Reprosentralen, University of Oslo

Abstract

Observations show that concentrations of atmospheric methane levelled off for about ten years until 2007, at which time the global methane concentrations started to increase again. While the reasons for this are not well understood, the cause of both the levelling and the increase could be due to emission changes, loss changes or a combination of the two. Oxidation by the hydroxyl radical is the most important methane sink, and if a reduction of this process is the reason for the resumed growth, the consequences could prove severe.

This thesis examines the importance of photodissociation of nitrogen dioxide and ozone for the hydroxyl radical concentration and methane lifetime. A counterfactual investigation was therefore conducted in order to answer two questions: How would the evolution of ozone, hydroxyl radical and methane concentrations and the lifetime of methane from 1850 to 2014 have looked if photodissociation of nitrogen dioxide or ozone happened less often? and Is it possible that one of the reactions is more important than the other with respect to the hydroxyl radical concentration and methane lifetime?

To answer these questions, three scenarios were simulated in the chemical transport model Oslo CTM3: two reduced reaction rate scenarios, with slowed photodissociation of, respectively, nitrogen dioxide and ozone, and one scenario with normal chemistry. All three scenarios were simulated for the years 1850 and 2014(pre-industrial and present-day).

Simulations showed that if either of the reaction rates is slowed, the concentration of the hydroxyl radical decreases even as the methane concentration increases. In both scenarios with slowed photodissociation, methane lifetime was found to be longer, and the increase in lifetime between 1850 to 2014 more prominent. The differences between the reduced reaction rate scenarios and the normal scenario, for ozone, hydroxyl radical and methane concentrations, were generally found to be more prominent in the northern hemisphere and at low to middle latitudes. The peak in vertical difference was generally found close to the surface.

The difference in the atmospheric lifetime of methane was found to increase more when photodissociation of ozone was reduced compared to nitrogen dioxide, a finding which implies that photodissociation of ozone is more critical to the hydroxyl radical concentration than photodissociation of nitrogen dioxide.

Oxidation by the hydroxyl radical is the most important methane sink and results from this thesis implies that slowing photodissociation rates for nitrogen dioxide or ozone would have a considerable impact on the methane lifetime.

Acknowledgements

This thesis would not exist without the great people around me.
To my supervisor, Terje Koren Berntsen, thank you for teaching me about atmospheric chemistry and making me realize how exciting this subject is.
Stefanie Falk, thank you for answering my every, more or less hopeless, technical question, taking time to explain and being so kind. Without you, there would not have been much after chapter two.
Denna, thank you for making time for proofreading and giving me such great advice on how to write clearly.
Ann Junita, thank you for converting my clumsy drawing into an excellent ozone figure.
Mamma, thank you for answering my every call and question and always taking my side. You are the wisest person I know, and I cannot imagine a better mother than you.
Pappa, Mona and Knut, thank you for always showing interest in what I am doing.
Anne-Li and Arnstein, I am so lucky to have you as my friends. You make me happy, even on the darkest day.
Finally, Vemund, thank you for enduring these years with me, you deserve a medal.

Dina Stabell
Oslo, August 2020

Contents

List of Figures

List of Tables

Chapter 1

Introduction

Methane is the second most important greenhouse gas(Myhre et al., 2013). Observations show that concentrations of methane levelled for about ten years until 2007, at which time the global methane concentrations started to increase again, for reasons not well understood(e.g., Turner et al., 2017; McNorton et al., 2016 and Nisbet et al., 2019). Because of its importance for climate change, understanding the reason for the resumed growth in concentration is of great importance. The reason for both the levelling and the increase could be due to emission changes, loss changes or a combination of the two. At the same time, as the methane concentration increased, methane's carbon isotope ratio has become more negative(Nisbet et al., 2016). This negative shift indicates a larger amount of ^{12}C to ^{13}C, which can give more insight into what has affected the methane concentration. Nisbet et al. (2016) have summarized three hypotheses, which are not mutually exclusive, for the renewed methane growth since 2007:

1. There has been an increase in biogenic emissions from very negative isotopic sources such as wetlands, ruminants and waste.

2. There has been a substantial rise in emissions from natural gas and oil use. For this to explain both the methane increase and the isotopic shift, either the fossil fuel emissions must be more isotopic negative, there must have been a decline in more isotopic positive emissions or a combination of the two.

3. The atmospheres oxidation capacity has declined.

Nisbet et al. (2016) also state that, *"If it is a sharp drop in the oxidative capacity, there are wide-ranging implications for many fields of atmospheric science that go far beyond greenhouse gas budget studies."*, and that the implications would be serious indeed. For this reason, the third hypothesis is the motivation to investigate what controls the atmospheric oxidation capacity. To be more specific, it is the tropospheric oxidation capacity which is under investigation, because the troposphere contains about 85% of the atmospheric mass(Jacob, 1999). The main contributor to the tropospheric oxidation capacity is the hydroxyl radical, which is the main sink for methane, carbon monoxide and other atmospheric trace gases(Jacob, 1999). Hypothesis 3 suggests that the atmosphere's oxidation capacity has declined, which would mean that the hydroxyl radical concentration has declined.

Until the late 1960s, scientists thought there was no significant production of hydroxyl radicals in the troposphere and that its tropospheric concentration was not sufficient to be important(Levy, 1973). This led to extensive concern regarding the tropospheric oxidation capacity as the emissions of trace gases that consumed it increased. The possibility of total depletion was considered a real problem, which would lead to toxic amounts of carbon monoxide in addition to immense climatic consequences. So, when it was discovered that there was, in fact, significant hydroxyl radical production in the troposphere(Levy, 1973, Levy, 1971), it was a massive relief. Even though there is a better understanding of the hydroxyl radical today compared to the 1960s, there are still uncertainties, and a better understanding of the processes controlling its abundance is needed(e.g., Naik et al., 2013 and Rigby et al., 2017).

Primary production of tropospheric hydroxyl radical is initiated by photodissociation of ozone to oxygen and electronically excited oxygen atoms. The electronically excited oxygen atom further reacts with water vapour to form two hydroxyl radicals. In other words, the reaction rate of this reaction and the abundance of ozone and water vapour are controlling factors for the hydroxyl radical production. Tropospheric ozone is also primarily produced within the troposphere, although stratospheric intrusion is a minor source as well. Production of tropospheric ozone takes place by photodissociation of nitrogen dioxide to nitrogen monoxide and atomic oxygen, where the latter further reacts with oxygen to produce ozone. Here it is seen that the reaction rate of the photodissociation reaction and the abundance of nitrogen dioxide is important for the production of tropospheric ozone, and hence the concentration of hydroxyl radicals which again controls the sink(and lifetime) of methane. In contrast to the hydroxyl radical and ozone, nitrogen oxide(nitrogen dioxide + nitrogen monoxide) is not mainly produced by chemical reactions but rather from direct emissions(Jacob, 1999).

1.1 Aim of Thesis

In summary, there are some main factors controlling the tropospheric oxidation capacity and hence the methane lifetime: photodissociation of ozone(O_3) and nitrogen dioxide(NO_2) and the tropospheric concentration of these two species. This thesis aims to investigate the importance of these two photochemical reactions for the concentration of ozone, the hydroxyl radical and methane *and* the lifetime of methane. The two reactions are expressed as follows:

$$NO_2 + hv \xrightarrow{\lambda 430nm} NO + O, \tag{R1}$$

$$O_3 + hv \xrightarrow{300nm < \lambda < 320nm} O_2 + O(^1D). \tag{R2}$$

How often these reactions take place in the troposphere can be altered by changing either the concentration of nitrogen dioxide or ozone *or* their reaction rates. This thesis presents a counterfactual investigation where the reaction rates are changed, with the objective of looking at the importance of the photochemical reactions (R1)-(R2). In conjunction with this objective, the following research questions are constructed:

1. What would the evolution, from pre-industrial to present day, of ozone, hydroxyl radical and methane concentrations and the lifetime of methane have looked if one of

the reactions (R1)-(R2) had a lower reaction rate in contrast to how that evolution has actually played out?

2. Is it possible that one of the two reactions, (R1)-(R2), is more important than the other with respect to the hydroxyl radical concentration and methane lifetime?

The motivation behind the first research question is the fact that the emissions of species with opposite effect on the hydroxyl radical concentration and methane lifetime, nitrogen dioxide, methane and carbon monoxide, have risen since the industrial evolution(e.g. Hoesly et al., 2018 and Dalsøren et al., 2016). These simultaneous changes, one boosting and the others consuming the hydroxyl radical, have ensured a quite stable hydroxyl radical concentration(Naik et al., 2013). However, if the change in emissions only for the methane concentration had occurred the situation would have been different. Considering the difference in effect of (R1)-(R2) to the hydroxyl radical concentration and methane lifetime, photodissociation of ozone(R2) is the primary production of the hydroxyl radical while photodissociation of nitrogen dioxide(R1) is important for production of ozone. When comparing these two reactions, the comparison is between the importance of ozone production and the ozone photodissociation to the hydroxyl radical concentration.

To answer the research questions, two experiments are carried out using the chemical transport model Oslo CTM3. In each experiment a reduced reaction rate scenario is simulated for the years 1850 and 2014. In addition simulations with normal reaction rates for the same years are conducted for comparison. In Experiment 1 the reaction rate of reaction R1 is reduced by 90%, while in Experiment 2 the reaction rate for reaction R2 is reduced by the same percentage.

1.2 Code Availability

The forked version of the Oslo CTM3 v1.1 used in this thesis is available on GitHub at `https://github.com/dinastabell/OsloCTM3`. Setup used for pre-industrial simulations are found in the branch *Pre-Industrial*, while for present-day simulations in *master*.

1.3 Outline of Thesis

This thesis consists of six chapters, including this. Chapter 2 presents theory of atmospheric chemistry needed for analyzing the results in addition to theory behind the Oslo CTM3. The settings used in Oslo CTM3, practical description of the experiments, preprocessing of data and the analysis methods are found in Chapter 3. Chapter 4 presents the results from the analysis, which are then discussed in Chapter 5. Finally, in Chapter 6 the answers to the research questions and proposals for future work are found.

Chapter 2

Theory

This chapter presents the relevant theory for this thesis. Section 2.1 explains the chemistry needed to understand and analyze the results from the two experiments in order to answer the research questions. In section 2.2 an introduction to the chemical transport model Oslo CTM3, which is used to simulate the experiments, is provided.

2.1 Chemistry

This section presents the relevant chemistry for understanding the importance of the photochemical reactions, and to be able to answer the research questions presented in Section 1.1. First, there is an explanation of some chemical terms; chemical families, radicals and hydrogen abstraction, and photodissociation. Following is an introduction to tropospheric ozone, hydroxyl radical, methane and nitrogen oxide. Finally, the changes in concentrations of the considered species and methane lifetime from 1850 to 2014 is presented.

The atmospheric concentration of chemical species is determined by how much production and loss there are. The sources for production are called *sources*, while the sources for loss are called *sinks*. The magnitude of the sources and the sinks are affected by many different processes. Therefore the introductions of ozone, hydroxyl radical and nitrogen oxide follow the same structure where first the sources are described followed by the sinks before finally a discussion on what affects their concentration. Tropospheric methane has a shorter introduction, focusing on its lifetime.

2.1.1 Chemical Families

In atmospheric chemistry, the term *chemical family* is used for groups of chemical species with rapid cycling amongst each other. This term is a useful tool if the lifetime of the family is longer than that of any individual family member. If this is the case, the family is a more conserved quantity in the atmosphere than the family members(Brasseur et al., 2017). Families encountered in this thesis are the nitrogen oxides, $NO_x \equiv NO_2 + NO$, and the odd oxygens, $O_x \equiv O_3 + O$. Here NO_x and O_x denotes the families while NO, NO_2, O_3, O denotes the family members. In these families, the oxygen atoms are transferred quickly **amongst** the family members but are more slowly lost **from** the family.

2.1.2 Radicals and Hydrogen Abstraction

It is generally considered common knowledge that radicals cause health problems by oxidizing human tissue and cause cancer. In the atmosphere, however, this oxidizing power is of great importance since many environmentally important trace gases are removed from the atmosphere mainly through oxidation (Jacob, 1999). The most important radical contributing to the oxidizing power of the troposphere is the hydroxyl radical, which has a central part in this thesis. In order to appreciate the importance of the hydroxyl radical, a clear understanding of chemical radicals is necessary. The octet rule is key; it says that, in general, atoms have a strong tendency to fill their valence shell with eight electrons(Reger et al., 2009). For the octet rule to hold in molecules, they have to have an even number of electrons, so that every electron can be in a pair. However, some molecules have an odd number of electrons, thereby breaking the octet rule. A *radical* is an atom or a molecule with at least one unpaired electron(Walling, 2018). Radicals react quickly with other atoms or molecules to be able to pair their unpaired electron and follow the octet rule. One way for them to do this is through *hydrogen abstraction*, a reaction in which the radical can be said to "steal" a hydrogen atom from another molecule.

2.1.3 Photodissociation

Photodissociation is a reaction where an incident photon breaks a chemical bond in a molecule, expressed as

$$\mathrm{X} + \mathrm{hv} \longrightarrow \mathrm{Y} + \mathrm{Z},$$

where X denotes the molecule which is being photodissociated, hv the incident photon and Y and Z the products of the reaction(Jacob, 1999). A *photon* is the smallest unit of electromagnetic radiation, and the sun is a source of this kind of radiation to the earth. Photons can be of different energies, which coincides with specific wavelengths.

A specific molecule only dissociates when the incident photon has the right amount of energy/ right wavelengths to break one of its chemical bonds. When describing photodissociation, the wavelength band needed is expressed by λ. For example, if the reaction only takes place for wavelengths less than 400nm, the reaction is expressed as:

$$\mathrm{X} + \mathrm{hv} \xrightarrow{\lambda < 400\mathrm{nm}} \mathrm{Y} + \mathrm{Z},$$

2.1.4 Tropospheric Ozone

In the stratosphere, ozone acts as protective gas by protecting life on Earth from harmful ultraviolet(UV) radiation from the sun. Tropospheric ozone has the same quality, however, the effects are not one-sided; in the free troposphere, ozone works simultaneously as a greenhouse gas and a precursor for the hydroxyl radical, thereby playing an important role not only for warming the planet but also removing other environmentally harmful trace gases. Ozone is toxic to life on Earth because it oxidizes biological tissue(Jacob, 1999), so ozone near the surface is unwanted. Figure 2.1 presents a schematic illustration of "good" and "bad" ozone. When "good" or "bad" ozone is referred to later in the text, it is to these definitions. The lifetime of tropospheric ozone is strongly dependent on season and location, and varies between a few days up to a year(Myhre et al., 2013).

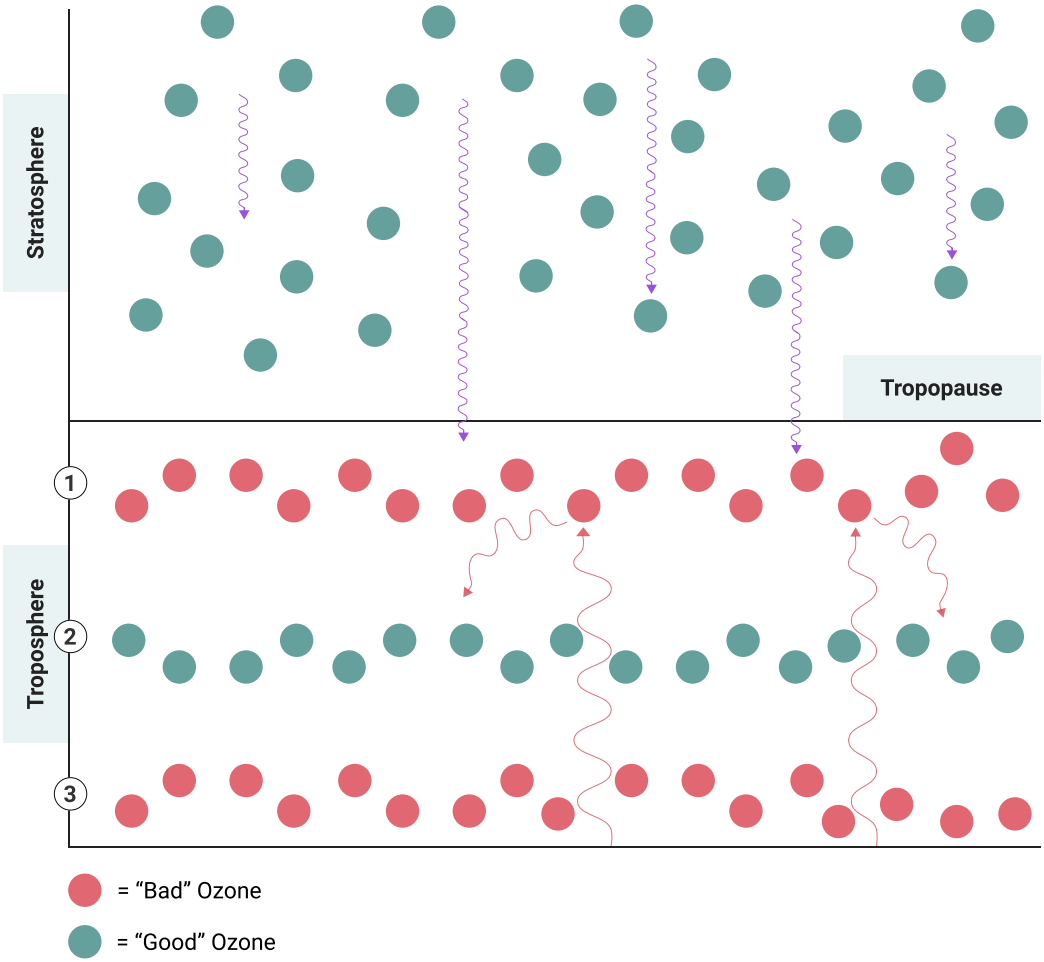

*Figure 2.1: Schematic illustration of tropospheric and stratospheric ozone. In the stratosphere, it protects life on earth from harmful ultraviolet(UV) radiation, in the upper troposphere(denoted as **(1)** on the y-axis) it acts as a greenhouse gas, in the mid-troposphere(denoted as **(2)** on the y-axis) it produces the hydroxyl radical, while near the surface(denoted as **(3)** it is an unwanted pollutant*

2.1.4.1 Ozone Sources

While stratospheric supply is a source of ozone(O_3) in the troposphere, chemical production is the main source. The primary tropospheric production of ozone is through photodissociation of nitrogen dioxide (NO_2). This process will now be described drawing upon Jacob (1999). Following are the reactions describing the photodissociation of nitrogen dioxide to ozone(where reaction (R3) can be recognized as reaction (R1) in Section 1.1):

$$NO_2 + hv \xrightarrow{\lambda < 430nm} NO + O, \tag{R3}$$

$$O + O_2 + M \longrightarrow O_3 + M, \tag{R4}$$

where M is an inert molecule which removes excess energy from the reaction.

The creation of ozone is initiated by production of hydroxyl radicals(described in Subsection 2.1.5.1), and propagated when these react with hydrocarbons(RH):

$$\mathrm{RH} + \mathrm{OH} \xrightarrow{\mathrm{O2}} \mathrm{RO_2} + \mathrm{H_2O}, \tag{R5}$$

where $\mathrm{RO_2}$ is an organic peroxy radical. The organic peroxy radical further reacts with nitrogen monoxide(NO), producing nitrogen dioxide and a organic oxy radical(RO):

$$\mathrm{RO_2} + \mathrm{NO} \longrightarrow \mathrm{RO} + \mathrm{NO_2}. \tag{R6}$$

The nitrogen dioxide molecule goes in to reaction R3 and produces ozone through reaction R4. What happens to the organic oxy radical differs, but typically a hydroperoxyl radical($\mathrm{HO_2}$) and a carbonyl($\mathrm{R'CHO}$) compound are produced:

$$\mathrm{RO} + \mathrm{O_2} \longrightarrow \mathrm{R'CHO} + \mathrm{HO_2}. \tag{R7}$$

Finally, the hydroperoxyl radical can react with nitrogen monoxide:

$$\mathrm{HO_2} + \mathrm{NO} \longrightarrow \mathrm{OH} + \mathrm{NO_2}, \tag{R8}$$

where again the nitrogen dioxide molecule goes into reaction R3. The resulting net equation is then given by:

$$\text{net: } \mathrm{RH} + 4\,\mathrm{O_2} \longrightarrow \mathrm{R'CHO} + 2\,\mathrm{O_3} + \mathrm{H_2O}. \tag{R9}$$

This reaction chain shows that nitrogen dioxide, and hence ozone, is produced by an organic peroxy radical and a hydroperoxyl radical through reactions (R6) and (R8) respectively. Note that nitrogen dioxide and nitrogen monoxide act as catalysts in the reaction chain, as non of them are net lost or produced. Methane($\mathrm{CH_4}$) is the simplest hydrocarbon, and following the reaction chain above, it can be seen that oxidation of methane in the presence of NO_x can produce ozone(see the *good result* example in Section 2.1.5.2).

In regimes with an abundance of NO_x, ozone is also produced by oxidation of carbon monoxide(CO), with the following net reaction:

$$\text{net: } \mathrm{CO} + 2\,\mathrm{O_2} \longrightarrow \mathrm{CO_2} + \mathrm{O_3} \tag{R10}$$

2.1.4.2 Ozone Sinks

Tropospheric loss of ozone takes place mainly by photodissociation, producing an excited oxygen atom($\mathrm{O(^1D)}$) which reacts with water to produce two hydroxyl radicals(Jacob, 1999):

$$\mathrm{O_3} + \mathrm{hv} \longrightarrow \mathrm{O_2} + \mathrm{O(^1D)} \tag{R11}$$

$$\mathrm{O(^1D)} + \mathrm{H_2O} \longrightarrow 2\,\mathrm{OH}. \tag{R12}$$

In environments with very low NO_x concentrations, hydroperoxyl and hydroxyl radicals can act as tropospheric ozone sinks through the following reactions:

$$\mathrm{HO_2} + \mathrm{O_3} \longrightarrow \mathrm{OH} + 2\,\mathrm{O_2} \tag{R13}$$

$$\mathrm{OH} + \mathrm{O_3} \longrightarrow \mathrm{HO_2} + \mathrm{O_2}. \tag{R14}$$

Dry deposition and loss to nitrogen dioxide during night(further discussed in Section 2.1.7.2) are important ozone sinks as well.

2.1.4.3 What is Affecting The Ozone Concentration?

Many things are affecting the abundance of ozone, and some of the interactions are complicated. This section will describe what is affecting the ozone concentration by explaining what affects ozone production(sources) and loss(sinks).

From reaction (R3) it is seen that the amount of solar insolation and concentration of nitrogen dioxide is important for ozone production. The amount of sunlight depends on the season and latitude, with more insolation occurring during summer and in low latitudes. Concentration of nitrogen dioxide depends on NO_x emissions and the oxidation of nitrogen monoxide to nitrogen dioxide; this is further explained in Section 2.1.7. From the reaction chain (R5)-(R8), it is evident that the abundance of hydroxyl radicals and hydrocarbons is also of great importance for oxidation of nitrogen monoxide to nitrogen dioxide, and hence to the concentration of ozone. What affects the abundance of hydroxyl radical will be discussed in Section 2.1.5.3. Emission sources for hydrocarbons are seen in Table 2.1.

The atmospheric lifetime of NO_x is short, on the order of about one day(Jacob, 1999). This short lifetime results in its spatial distribution being highly variable, with a higher incidence occuring closer to the source of emission. For this reason, the NO_x emission source plays an important role in determining whether it leads to "good" or "bad" ozone(schematically illustrated in Figure 2.1). Emission sources at or close to the Earth's surface, such as biomass burning, fossil fuel combustion and soils, leads to the "bad" ozone, which is damaging to biological tissue. NO_x emitting sources in the free troposphere, such as aircraft and lightning, leads to the "bad" ozone which acts as a greenhouse gas and "good" ozone which produces the hydroxyl radical.

The ratio between NO_x and hydrocarbons is also an important factor for ozone production. In NO_x-limited environments, the ozone production is independent of the hydrocarbon emissions and varies linearly with NO_x emissions. In hydrocarbon-limited environments, the ozone production increases linearly with hydrocarbon concentrations and inversely with NO_x concentrations(Jacob, 1999). The ideal combination for maximal ozone production is when the NO_x emissions are about twice as large as the hydrocarbon emissions.

Ozone production efficiency is also a complicating factor and is conceptually defined as the number of ozone molecules produced per molecule of NO_x consumed(Jacob, 1999). In NO_x-limited environments, the production becomes more efficient with increasing hydrocarbon concentrations and becomes less efficient with increasing NO_x concentration. When the hydrocarbon concentration increases, the hydroxyl radical concentration decreases as a result of reaction R5. This leads to an increased NO_x lifetime, which again allows each emitted NO_x molecule to produce more ozone; a result of increased ozone production efficiency. If, on the other hand, it is the NO_x concentration which increases, the hydroxyl radical concentration will increase by reaction (R12), which will lower the ozone production efficiency. This negative dependency dampens the ozone decrease expected from a given NO_x reduction.

Solar insolation and NO_x concentrations play an important role in the magnitude of ozone sinks as well. Photodissociation through reaction (R11) is the largest ozone sink in the troposphere. This means that the amount of solar insolation is important not only for ozone production but also for ozone loss, resulting in higher ozone production and loss in the summer as well as at low latitudes(Lelieveld et al., 2016). The insolation

Species	Natural	Anthropogenic
hydrocarbons	terrestrial vegetation	combustion, fuel evaporation, solvent use, chemical manufacturing

Table 2.1: Emission sources for hydrocarbons(Jacob, 1999), divided into natural and anthropogenic emission sources.

needed photodissociation of ozone lays in a very narrow wavelength band and how much insolation with right wavelengths penetrates through to the troposphere depends on the amount of ozone in the stratosphere, because the stratospheric ozone photodissociates using the same wavelengths. In the tropics, the stratospheric ozone layer is relatively thin, allowing more UV radiation to penetrate through to the troposphere, which can then contribute to ozone loss.

In contrast to ozone production, low NO_x concentrations are advantageous for ozone loss; in low-NO_x environments hydroperoxyl and hydroxyl radicals can act as ozone sinks, as seen in reactions (R13)-(R14).

2.1.5 Tropospheric Hydroxyl Radical

The hydroxyl radical is the most important oxidant in the troposphere and is the main sink for methane. It reacts quickly with molecules containing hydrogen due to hydrogen abstraction which converts the hydroxyl radical to water. The lifetime of the hydroxyl radical is on the order of one second, resulting in a highly spatial variable concentration. Its atmospheric concentration is very low. The short lifetime and low concentration make it extremely difficult to accurately measure global hydroxyl radical concentrations. Methyl chloroform concentrations have been used to estimate the mean global hydroxyl radical concentration. The only emissions of methyl chloroform are anthropogenic, making it easy to measure the emissions, and oxidation by the hydroxyl radical is its main sink(Jacob, 1999). However, methyl chloroform was banned by the Montreal Protocol in 1987, making its current concentration very low with further emissions difficult to determine(Krol et al., 2003). Other trace gases are being examined for estimating hydroxyl radical concentrations for more accurately. Pending further studies in this field, the available methods for finding the global hydroxyl radical concentration are either by using methyl chloroform measurements or through estimations made by atmospheric chemical tracer models.

2.1.5.1 Hydroxyl Radical Sources

In the troposphere, the primary source of hydroxyl(OH) radicals is through photodissociation of ozone in the very narrow wavelength band between 300 and 320nm (Jacob, 1999):

$$O_3 + h\nu \xrightarrow{300 < \lambda < 320nm} O_2 + O(^1D) \quad \text{(R15)}$$

$$O(^1D) + H_2O \longrightarrow 2\,OH. \quad \text{(R16)}$$

Additionally, recycling mechanisms are secondary sources of the hydroxyl radical, in which it is first used in an oxidation process and, later in the reaction chain, produced or recycled. These recycling mechanism are called the *NO_x recycling mechanism* and the *O_x recycling mechanism*, which are now described following Lelieveld et al. (2016). Considering first the oxidation of carbon monoxide, which uses a hydroxyl radical:

$$\mathrm{CO + OH \longrightarrow CO_2 + H} \tag{R17}$$
$$\mathrm{H + O_2\,(^+M) \longrightarrow HO_2 + M.} \tag{R18}$$

The product of interest here is the hydroperoxyl radical, and what happens to it depends on the environment in which the reactions take place. In high-NO_x environments the NO_x recycling mechanism takes place through the following reaction:

$$\mathrm{NO + HO_2 \longrightarrow NO_2 + OH.} \tag{R19}$$

The resulting nitrogen dioxide will produce ozone, through reactions (R3)-(R4), which leads to additional primary hydroxyl radical production through reactions (R15)-(R16).

If, on the other hand, the carbon monoxide oxidation(R17-R18) takes place in a low-NO_x environment, the hydroperoxyl radical can go through the O_x recycling mechanism. In the O_x recycling mechanism the hydroperoxyl radical can either react with ozone

$$\mathrm{O_3 + HO_2 \longrightarrow 2\,O_2 + OH,} \tag{R20}$$

or another hydroperoxyl radical

$$\mathrm{HO_2 + HO_2 \longrightarrow H_2O_2 + O_2} \tag{R21}$$
$$\mathrm{H_2O_2 + hv \xrightarrow{\lambda< 550nm} 2\,OH.} \tag{R22}$$

2.1.5.2 Hydroxyl Radical Sinks

Hydroxyl radicals are lost from the troposphere through acting as an oxidant in reactions with various atmospheric gases. The largest sink for the hydroxyl radical is through oxidation of carbon monoxide, as shown in reaction R17. Loss through oxidation of methane follows closely in importance(Jacob, 1999) and is described by the following reactions:

$$\mathrm{CH_4 + OH \longrightarrow CH_3 + H_2O} \tag{R23}$$
$$\mathrm{CH_3 + O_2 + M \longrightarrow CH_3O_2 + M.} \tag{R24}$$

How this oxidation mechanism continues depends on the environment in which it happens. However, the end product always contains water vapour and a carbon dioxide molecule, which also are potent greenhouse gases(Jacob, 1999). How good or bad the result is, concerning the hydroxyl radical, largely depends on whether there are nitrogen oxide(NO_x) present or not. Two extreme examples, following Jacob (1999), illustrate this dependency.

The "good result" example: Assuming an environment high in nitrogen oxide, and some luck, the methane oxidation can proceed as follows:

$$CH_3O_2 + NO \longrightarrow CH_3O + NO_2, \tag{R25}$$

where the nitrogen dioxide molecule can go into reaction (R3)-(R4) to produce ozone. The resulting methoxy radical(CH_3O) now reacts with oxygen, to produce formaldehyde(CH_{20}):

$$CH_3O + O_2 \longrightarrow CH_2O + HO_2, \tag{R26}$$

where the hydroperoxyl radical molecule goes into reaction (R19) to produce nitrogen dioxide and hydroxyl radical. The produced nitrogen dioxide can again react through reaction (R3)-(R4). At this point, the formaldehyde molecule goes through photodissociation:

$$CH_2O + hv \xrightarrow{O2} CHO + HO_2, \tag{R27}$$

where the hydroperoxyl radical reacts as described in reaction (R19), resulting in a hydroxyl radical and an ozone molecule. The formyl radical(CHO) further reacts with oxygen:

$$CHO + O_2 \longrightarrow CO + HO_2. \tag{R28}$$

The hydroperoxyl radical continues as previously, resulting in an additional hydroxyl radical and ozone molecule, while the carbon monoxide(CO) continues to oxidize to carbon dioxide(CO_2):

$$CO + OH \longrightarrow CO_2 + H \tag{R29}$$
$$H + O_2 + M \longrightarrow HO_2 + M. \tag{R30}$$

The resulting net equation is then given by

$$\text{net: } CH_4 + 10\,O_2 \longrightarrow CO_2 + H_2O + 5\,O_3 + 2\,OH, \tag{R31}$$

The "bad result" example: Assuming an environment depleted of NO_x, the methane oxidation can proceed as follows:

$$CH_3O_2 + HO_2 \longrightarrow CH_3OOH + O_2 \tag{R32}$$
$$CH_3OOH + OH \longrightarrow CH_2 + OH + H_2O \tag{R33}$$
$$CH_3 + OH \longrightarrow CHO + H_2O \tag{R34}$$
$$CHO + O_2 \longrightarrow CO + HO_2 \tag{R35}$$
$$CO + OH \longrightarrow CO_2 + H \tag{R36}$$
$$H + O_2 + M \longrightarrow HO_2 + M. \tag{R37}$$

The net reaction for this relatively straightforward reaction chain is expressed by:

$$\text{net: } CH_4 + 3\,OH + 2\,O_2 \longrightarrow CO_2 + 3\,H_2O + HO_2. \tag{R38}$$

In order to explain what makes *the good result example* good and *the bad result example* bad with respect to the hydroxyl radical, their net reactions (R31) and (R38) must be compared: First, in reaction (R31), two hydroxyl radicals are produced, while in reaction (R38) three are used. Second, in reaction (R31), there are five ozone molecules produced, which by reactions (R15)-(R16) would produce ten additional hydroxyl radicals. Finally in reaction (R38), there are three water vapour molecules produced compared to (R31) which produces only one. Water vapour could be either good or bad; in environments where ozone photodissociates, it could contribute to the production of hydroxyl radical, but on the other hand, it is a strong greenhouse gas. Looking at the environments in which *the bad result example* takes place(depleted of NO_x), there is most likely not much ozone present(see Section 2.1.4.3), so the benefits of water vapour would be negligible.

As noted, these are two extreme examples, and results somewhere in between are more likely. However, it is essential to remember that oxidation of methane is the second-largest hydroxyl radical sink.

In very high NO_x environments, NO_x can also be a large hydroxyl radical sink through the reaction:

$$NO_2 + OH + M \longrightarrow HNO_3 + M, \tag{R39}$$

where M is is an air molecule that removes excess energy from the reaction(Lelieveld et al., 2016).

2.1.5.3 What is Affecting the Hydroxyl Radical Concentration?

This section gives a summary of what is affecting the tropospheric hydroxyl radical concentration by looking at what controls the magnitude of its sources and sinks.

As seen from reaction (R15)-(R16) the amount of ozone, solar insolation and water vapour is of great importance for hydroxyl radical production. What affects the ozone concentration and the solar insolation was discussed in Section 2.1.4.3. Atmospheric water vapour concentration is controlled by temperature and the amount of water available to evaporate. Temperature is vital because warmer air can hold more water vapour than cold air(Lamb et al., 2011). For these reasons, the water vapour concentrations are expected to be higher in moist regions, such as over oceans and with high temperatures. In the tropics, the ozone layer is relatively thin, allowing more UV radiation to penetrate to the troposphere, resulting in high insolation and water vapour concentration(Lelieveld et al., 2016). This results in the most significant hydroxyl radical production taking place in the tropics. In the troposphere, the UV radiation increases with altitude, while water vapour concentration decreases, leading to a peak hydroxyl radical production in the middle troposphere(Jacob, 1999).

Looking at the recycling mechanisms for secondary hydroxyl radical production, it is evident that for NO_x recycling (R19) the NO_x concentration is important. In the O_x recycling mechanism(R20-R22), the concentrations of ozone and hydroperoxyl radical, and solar insolation is important for the hydroxyl radical recycling. NO_x emission sources are listed in Table 2.2 and discussed in Section 2.1.7, while what affects the ozone concentration is discussed in Section 2.1.4.3.

The abundance of some trace gases is of great importance to the hydroxyl radical loss. Oxidation of carbon monoxide is the largest tropospheric hydroxyl radical sink.

Carbon monoxide is emitted by fossil fuel combustion, burning of biomass, vegetation, oceans and oxidation of methane and other hydrocarbons(Jacob, 1999). Exactly how much these oxidation processes lead to hydroxyl radical loss largely depends on the amount of NO_x present during the process. This effect is exemplified through the NO_x recycling mechanism and the good/bad result examples in Subsection 2.1.5.2.

An important fact to note is that the gases important for hydroxyl radical production and loss have different atmospheric lifetimes. The production of hydroxyl radical is largely dependent on NO_x and ozone, which are short-lived gases. These factors make the production most prominent in the emission regions of these gases. Carbon monoxide and methane, which are the most important hydroxyl radical sinks, on the other hand, are long-lived gases which are well mixed in the troposphere. This combination makes the hydroxyl radical concentration highly spatially variable.

2.1.6 Tropospheric Methane

Methane is the second most important greenhouse gas after carbon dioxide. The radiative forcing of methane is much higher than that of carbon dioxide, however, and luckily for human life on Earth, its lifetime is much shorter(approximately 9.1 years(Ciais et al., 2013)). Despite methane having a short lifetime relative to carbon dioxide, its lifetime is sufficient for it to be categorized as a *well-mixed greenhouse gas* (WMGHG): a greenhouse gas which has a lifetime long enough for its geographical concentration to be about the same everywhere(Myhre et al., 2013).

The global warming potential of methane has a value for 100 years, 28 times that of carbon dioxide(Myhre et al., 2013), so determining the lifetime of methane is important for quantifying its climate impact. The lifetime of an atmospheric species is defined as the average time a molecule of the species exists in the atmosphere. Methane's tropospheric lifetime can be calculated by the ratio between the mass of tropospheric methane to the removal rate(Jacob, 1999):

$$\tau = \frac{m_{CH_4}}{\text{removal rate}}. \tag{2.1}$$

The removal rate of methane depends on the magnitude of the sinks. Oxidation by the hydroxyl radical is the largest methane sink in the atmosphere and accounts for about 90% of the total loss. In addition, methane also has other smaller sinks through photochemistry both in the stratosphere and the marine boundary layer, as well as in soil(Saunois et al., 2016). Oxidation by the hydroxyl radical is the focus of this thesis, described in Section 2.1.5.2. Therefore it is specifically the lifetime of methane to this sink which are of interest:

$$\tau = \frac{m_{CH_4}}{\text{removal by OH radical}}. \tag{2.2}$$

A change in methane lifetime leads to a change(with same sign) in methane concentration, and this changes the hydroxyl radical concentration, which again changes the lifetime further in the same direction as the initial change(Myhre et al., 2013). For Example; if the methane lifetime increases, the methane concentration increases, this leads to a decrease in hydroxyl radical concentration which again makes the methane lifetime increase. Estimations of the current methane lifetime to oxidation by the hydroxyl radical among the ACCMIP models is 9.8±1.6 years(Voulgarakis et al., 2013).

2.1.7 Tropospheric Nitrogen Oxide

When nitrogen oxide(NO_x) is mentioned in the news, the context is usually air pollution and the need to cut the emissions. In the perspective of the tropospheric oxidation capacity, as evident from Section 2.1.4 and 2.1.5, NO_x plays an important role in sustaining this capacity. The lifetime of NO_x is about one day, leading to high spatial variations, with the highest concentrations close to the emission regions(Jacob, 1999). Because of this short lifetime, the effect of NO_x is dependent on where in the troposphere it is emitted. When emitted close to the surface, it leads to the production of toxic surface ozone(schematically illustrated in Figure 2.1). NO_x further up in the troposphere, on the other hand, leads to the "good" ozone which produces hydroxyl radicals. Additionally, NO_x plays an important role for how many hydroxyl radicals are produced/used during oxidation of trace gases, as exemplified in the good/bad result example in Section 2.1.5.2. This section describes the NO_x concentration by its sources and sinks.

2.1.7.1 Tropospheric Nitrogen Oxide Sources

NO_x is primarily produced as nitrogen monoxide, but oxidizes quickly into nitrogen dioxide(Delmas et al., 1997), and as described in Section 2.1.1, there is a rapid cycling between nitrogen monoxide and nitrogen dioxide. This tropospheric NO_x cycling takes place on a timescale of a single minute during daytime by reactions (R40) through (R42)(Jacob, 1999):

$$HO_2 + NO \longrightarrow OH + NO_2, \tag{R40}$$

$$NO + O_3 \longrightarrow NO_2 + O_2, \tag{R41}$$

$$NO_2 + hv \xrightarrow{O2} NO + O_3. \tag{R42}$$

Reaction (R42) requires sunlight, so during night, NO_x exists exclusively as nitrogen dioxide.

The sources of NO_x are shown in Table 2.2, where fossil fuel combustion and biomass burning are the largest contributors(Jacob, 1999). Because these sources are close to the Earth's surface, the effects of the NO_x they produce are primarily in the region of those sources. Emissions from lightening, ammonia oxidation, transport from the stratosphere and aircraft exhaust, on the other hand, take place in the free troposphere. Here the lifetime of NO_x is longer, and the effect on the oxidation capacity is significant, even though the emissions are small(Delmas et al., 1997).

Species	Natural	Anthropogenic
NO_x	biomass burning, soils, lightning, NH_3 oxidation, transport from the stratosphere	fossil fuel combustion, biomass burning, aircraft exhaust

Table 2.2: Emission sources for NOx (Jacob, 1999), divided into natural and anthropogenic emission sources.

Lightening is the dominant source for the free tropospheric NO_x(Delmas et al., 1997), where the high temperature involved thermolyzes O_2(following Jacob, 1999):

$$O_2 \xleftrightarrow{\text{heat}} O + O. \tag{R43}$$

The atomic oxygen that is produced further reacts with nitrogen(N_2) and produces nitrogen dioxide

$$O + N_2 \longleftrightarrow NO + N, \tag{R44}$$

where the atomic nitrogen reacts with oxygen to produce nitrogen monoxide:

$$N + O_2 \longleftrightarrow NO + O. \tag{R45}$$

With the high temperatures in the lightning, the equilibria, (R43)-(R45), shifts to the right, promoting nitrogen monoxide formation.

2.1.7.2 Tropospheric Nitrogen Oxide Sinks

In this section the NO_x sinks are described following Jacob (1999). The main NO_x sink is oxidation to nitric acid(HNO_3). This oxidation occurs through by different reactions depending on the time of day. During the day, the oxidation is through,

$$NO_2 + OH + M \longrightarrow HNO_3 + M \tag{R46}$$
$$\tag{R47}$$

while at night,

$$NO_2 + O_3 \longrightarrow NO_3 + O_2, \tag{R48}$$
$$NO_3 + NO_2 + M \longrightarrow N_2O_5 + M, \tag{R49}$$
$$N_2O_5 + H_2O \xrightarrow{\text{aerosol}} 2\,HNO_3. \tag{R50}$$

Nitric acid is highly soluble in water, so it is scavenged by precipitation which results in varying lifetimes depending on its location in the troposphere. In the lower troposphere, the lifetime is a few days, while in the upper troposphere it is a few weeks.

2.1.7.3 What is Affecting the Nitrogen Oxide Concentration?

This section will sum up what is affecting the NO_x concentration by its sources and sinks. In addition, what affects the ratio between nitrogen dioxide and nitrogen monoxide is considered.

The magnitude of the sources is determined by the magnitude of the emission processes described in Table 2.2. However, some important factors are affecting the natural NO_x sources. Lightning is the most important natural source considering hydroxyl radical formation, and the frequency of lightning depends on many factors, some being; temperature, water vapour content in the air and topography(The National Severe Storms Laboratory, n.d.). Besides, lightning strokes is one of the main factors controlling natural biomass burning(Krause et al., 2014). During the daytime, the magnitude of the NO_x sink depends on the abundance of hydroxyl radicals, while at nighttime the abundance of ozone.

What affects the abundance of hydroxyl radicals and ozone is described, respectively, in Section 2.1.5.3 and 2.1.4.3.

NO_x consists of nitrogen dioxide and nitrogen monoxide, and as aforementioned the cycling between them takes place on the timescale of one minute. In the cycling process, Reaction (R40)-(R41), hydroperoxyl radical and ozone concentrations and solar insolation are important factors. If one, or more, of these factors are changed, the cycling process can slow down favoring either nitrogen dioxide or nitrogen monoxide. For example, if the ozone concentration decreases, reaction (R41) will happen less often, and the ratio between nitrogen dioxide and nitrogen monoxide could shift in favour of nitrogen monoxide.

2.1.8 Change in Concentrations From Pre-Industrial to Present Day

In this thesis, the change and difference in change of ozone, hydroxyl radicals, methane and nitrogen dioxide concentrations between the year 1850 and 2014 are considered. This section presents concentrations and changes in the aforementioned species, from pre-industrial to present-day, found in other studies.

Table 2.3 shows the burden of ozone, hydroxyl radical and methane, and methane lifetime in the years 1850 and 2000 and the percentage change between the two years. The result shows that the burden of ozone and methane and the methane lifetime has increased from 1850 to 2014 has increased, while the hydroxyl radical concentration and methane lifetime has decreased. Emissions of NO_x have also increased from pre-industrial times to present-day, from close to zero in 1850 to almost 150Tg/year in 2014(Hoesly et al., 2018). The present day emissions of NO_x are largest in Asia(Gaudel et al., 2018).

	Ozone burden(Tg)	Hydoxyl radical burden(Tg)	Methane burden(Tg)	Methane lifetime(years)
1850	239	11.3	2179	10.1
2000	322	11.1	4813	9.7
% change	+35%	-1.8%	+120%	-4%

Table 2.3: Burden of ozone, hydroxyl radical and methane, and methane lifetime in the years 1850 and 2000 and the percentage change between the two years. These are results from multi-model means from the Atmospheric Chemistry and Climate Model Intercomparison Project(ACCMIP) models(Naik et al., 2013 and Young et al., 2013).

2.2 Oslo CTM3

The Oslo CTM3 is an offline three-dimensional global chemical transport model(CTM), first developed at the Department of Geosciences at the University of Oslo and later at the Center for International Climate Research (CICERO). A CTM can be offline or online. The difference is that an offline model does not generate its own meteorological environment, but rather use one created by an external meteorological model. In contrast, an online model is integrated into a parent meteorological model(Brasseur et al., 2017). In this thesis, the Oslo CTM3 is used for simulating different atmospheric chemical

experiments which are further described in Section 3.3. This section provides a short introduction to chemical transport modeling, then discusses the Oslo CTM3 and the theory behind it.

2.2.1 What is a Chemical Transport Model?

A chemical transport model(CTM) is a model which simulates evolution of the chemical species in the atmosphere. These models are a handy tool because they can be used to simulate the future state of the atmosphere as well as atmospheric experiments(Brasseur et al., 2017).

Explained very simply, a CTM simulation is performed by first providing the model with information on the state of the atmosphere as the starting point of the simulation. From this point, the model solves physical and chemical equations to simulate how the state of the atmosphere evolves from the given initial state. The output of the model is the simulated concentrations and distributions of the included chemical species in a given time interval since the beginning of the simulation. A simple flowchart showing this can be seen in Figure 2.2.

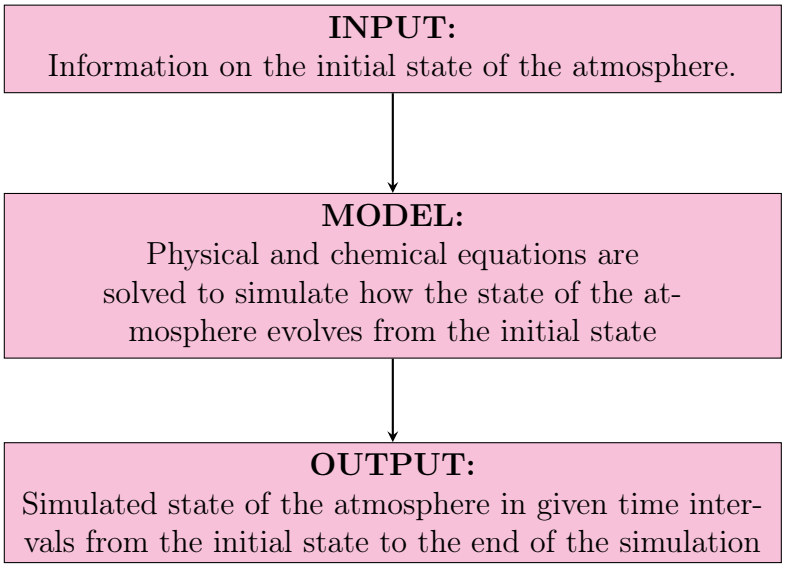

Figure 2.2: Schematic illustration of a chemical transport model

Compositions of chemical species in a CTM can be described either by the Eulerian or Lagrangian method. An Eulerian model describes the atmospheric composition within fixed grid boxes through which the air flows. In contrast, a Lagrangian model describes the composition of one or more air plumes moving with the airflow(Jacob, 1999). Oslo CTM3 is an Eulerian model and what follows is an example of how the composition of one chemical species in an Eulerian model is described, drawn upon Jacob (1999).

Consider a volume(box) of air with a chemical concentration(m1) of one chemical species, X. Assume that this box is surrounded by four other boxes of air, where their chemical concentrations of X are given by m_2, m_3, m_4, m_5. The value of interest is the concentration m_1 of X. This concentration is determined by the following processes: emissions(E), chemical production(P), chemical loss(L), deposition(D) and transport

into(F_{in}) and out of(F_{out}) the given volume of air. To calculate the time evolution of m_1, the mass balance equation is used

$$\frac{dm_1}{dt} = E + P + F_{in} - L - D - F_{out}. \tag{2.3}$$

In this example, with four surrounding volumes of air, the transport contributing to m_1 is the sum $F_{in} = F_{2\to1} + F_{3\to1} + F_{4\to1} + F_{5\to1}$, and the transport out of the box F_{out} is the same sum, but with the arrows shifted to the left.

2.2.2 Transport

Transport of atmospheric species in the Oslo CTM3 is performed through three different schemes: large-scale advection, convection and boundary layer mixing(Haslerud, 2018), and driven by 3-hourly meterological forecast data from the European Center for Medium-range Weather Forecasting (ECMWF) Integrated Forecast System (IFS).

Second Order Moments (SOM) scheme is the basis for the large scale advection. SOM is a nondiffusive method for three-dimensional advection of trace species introduced in 1986 (Prather, 1986) and improved in 2008 (Prather et al., 2008). In the SOM scheme, found in the script *p-dyn0.f*, transport of tracers from the zonal(U) and meridional(V) meteorological fields are calculated first, before using these to calculate the convergence of air in each layer and finally calculate the vertical field(W).

The EMCWF IFS convective scheme (Tiedtke, 1989) which is used to calculate convection through the use of mass fluxes of updrafts and downdrafts, is found in the script *convection.f90*.

Boundary layer mixing can be calculated either by the Prather bulk scheme or the Holtslag k-profile scheme(Holtslag et al., 1990), the decired scheme is selected through the variable *NBLX* in the input file. The boundary layer mixing takes place before chemistry each chemical timestep, which is usually 15 minutes. Some atmospheric species have atmospheric lifetimes much shorter than these 15 minutes, such as the hydroxyl radical, which is of great importance in this thesis. The concentration of these short-lived species may change considerably between one transport timestep and the next; the Oslo CTM3 solves for this by dividing the transport into transported and non-transported species.

2.2.3 Solving the Mass Balance Equation for Chemical Kinetics

The mass balance equation for chemical kinetics is similar to Equation 2.3, but only including the chemical production and loss(Haslerud, 2018):

$$\frac{dm}{dt} = P - Lm. \tag{2.4}$$

The chemical reactions contributing to the production P and the loss L have different rate constants, resulting in a set of differential equations with different time constants. Such a set of differential equations are called a stiff system.

In Oslo CTM3 these calculations have to be solved for all included species, in every grid box each timestep in the simulation. In other words, the calculations are repeated a large number of times. This section describes the two methods used for solving these equations, in a computationally cheap way; the quasi-steady-state approximation and the family solution.

2.2.3.1 Quasi-Steady-State Approximation Chemical Integration

The quasi-steady-state approximation(QSSA) is a mathematically simple method, but the error bounds are difficult to estimate. However, as noted, since the integrations are repeated a large number of times, this computationally cheaper method is favourable(Hesstvedt et al., 1978).

The QSSA method, as described by Hesstvedt et al. (1978), is based on the mass balance equation for chemical kinetics (Eq. 2.4). It is assumed that P and L are constant over a time interval, Δt, which is the step length in the numerical integration. Then equation 2.4 can be solved analytically, and the concentration at the next time step($t+\Delta t$) is expressed as

$$m_{t+\Delta t} = \frac{P}{L} + (m_t - \frac{P}{L})e^{(-L\Delta t)}, \tag{2.5}$$

where P/L is the chemical equilibrium concentration.

The chemical lifetime of a component is defined as $\tau = 1/L$. From these lifetimes, the species are classified in three categories; shortlived($\tau < \Delta t/10$), intermediate($\Delta t/10 \leq \tau \leq 100\Delta t$) and long-lived($\tau > 100\Delta t$). Species with a short lifetime have a large chemical loss L (this is why their lifetime is short), while the long-lived species, on the other hand, have a small chemical loss. Due to the differences in the magnitude of L, the equations for the three categories can be expressed differently(Haslerud, 2018):

1. Shortlived species: For these species the loss L is large, so $e^{(-L\Delta t)}$ can be approximated to zero, resulting in the following expression

$$m_{t+\Delta t} = \frac{P}{L}. \tag{2.6}$$

   Note that this expression describe chemical equilibrium.

2. Intermediate species: These species are solved by the use of the full equation 2.5.

3. Longlived species: The loss L for these species, so $e^{(-L\Delta t)}$ can be approximated as $1 - L\Delta t$, resulting in the following expression

$$m_{t+\Delta t} = m_t + (\frac{P}{L} - m_t)L\Delta t. \tag{2.7}$$

2.2.4 Atmospheric Chemistry

The Oslo CTM3 contains a tropospheric and a stratospheric chemistry routine. It can be run with either just the tropospheric routine or both, but the stratospheric routine can not be run without the tropospheric(Haslerud, 2018). This section describes how tropospheric and stratospheric chemistry and photochemistry is carried out in the model.

2.2.4.1 Tropospheric Chemistry

The tropospheric chemistry routine, in its general form, contains 46 chemical species and is in principle a 1D model looping through a column. The tropopause is set differently depending on whether the stratosphere is included or not. When the stratosphere is included, the model finds the tropopause for each grid box, while when not included tropospheric chemistry is calculated to a given altitude(Haslerud, 2018).

Transport from the stratosphere to the troposphere is essential for some chemical species, for example, ozone and NO_x which are of great importance in this thesis. When the stratosphere is not included, these are set from the climatology of a full-chemistry simulation for the years 2000-2008. Transport of chemical species from the troposphere to the stratosphere is not dependent on whether the stratospheric routine is included or not(Haslerud, 2018).

As mentioned in Section 2.2.2 some species have a lifetime much shorter than the transporting time step, and their tracer concentration may change considerably between one transport timestep and the next. However, some of these species are still transported in the model, even though their historical value is of little value. The hydroxyl radical is one of these species, but it might not be a big problem to transport it due to the iteration to get a stable value(Haslerud, 2018)

In the Oslo CTM3, there are two options for surface methane; it can be a fixed field or surface emissions can be included. If choosing the fixed methane field, it is critical to scale for the year of interest, especially when running pre-industrial simulations. When including the surface emissions currently, the only possible set-up is a combination of anthropogenic emissions and natural emissions and soil uptake(Haslerud, 2018).

2.2.4.2 Stratospheric Chemistry

The stratospheric chemistry in its general form contains 46 chemical species and is defined from the tropopause level to the uppermost vertical grid box. To be able to work, this routine needs input giving information about stratospheric background aerosols and boundary conditions for the species treated only in the stratosphere. A fitting tracer list with the correct number of species is also needed(Haslerud, 2018).

When the stratospheric routine is not included, as mentioned in Section 2.2.4.1, transport into/out of the stratosphere still takes place. However, when species are transported into the stratosphere, no actual chemistry is applied. In this case, the climatology mentioned in Section 2.2.4.1 is also used here. This will affect the photochemistry as well.

Stratospheric H_2O is calculated by the following equation

$$H_2O = \sum H_2 - 2\,CH_4 - H_2. \tag{2.8}$$

Here $\sum H_2$ denotes the sum of potential hydrogen, and is set as a constant in the mode which has to be scaled if running pre-industrial simulations(Haslerud, 2018).

2.2.4.3 Photochemistry

Photodissociation was described in Section 2.1.3, and this section will describe how this is treated in the Oslo CTM3. The fast-JX method, version 6.7c, is used to calculate the photodissociation rates in Oslo CTM3. Fast-JX is an online method which calculates the

photodissociation rates in both the troposphere and the stratosphere. In the troposphere 20 rates are calculated, while in the stratosphere there are 49. The ozone column is used to calculate the radiative properties, and a climatology is applied to account for the atmosphere above the model(Haslerud, 2018). Photodissociation rates depend on solar flux, cloud cover and aerosols. Solar flux is calculated from the Solar Spectral Irradiance Monitor by taking the average of solar low and 80% of solar high. If there are clouds present in a model column, the clouds optical properties can be calculated either by averaging the cloud cover in a grid box or by using random cloud cover.

2.2.5 Resolution

The native meteorological data from ECMWF IFS has the horizontal resolution 1.125°x 1.125°(T159). Oslo CTM3 can be run with the native meteorological resolution or with degraded resolution combining 2 or 4 native grid boxes into one, as summarized in 2.4. The vertical resolution of the meteorological data is available in both 40- and 60-layer versions. In the model, there is also an option to collapse the vertical resolution, where layer 1-3 and layer 4-5 is combined into two layers. The vertical grid in the model is not fixed throughout a model run but depends on the pressure of the meteorological input(Haslerud, 2018).

Resolution options	Resolution (degrees)	Model option (HWINDOW)
Native resolution	1.125°x 1.125°	HORIGINAL
Combine 2x2 native boxes	2.25°x 2.25°	HTWO
Combine 4x4 native boxes	4.5°x 4.5°	HFOUR

Table 2.4: Resolution options in Oslo CTM3

Chapter 3

Method

In this thesis, the Oslo CTM3 is used to simulate scenarios to investigate the importance of photochemical reactions to the concentration of ozone, hydroxyl radical, methane and nitrogen dioxide. This chapter first explains how the Oslo CTM3 is run and set up in the simulations before the preprocessing, and the analysis methods are explained.

3.1 Supercomputer

The Oslo CTM3 requires large amounts of data and computing power making it infeasible to run the model on a personal computer. Therefore, a high-performance computing(HPC) computation cluster(also known as a supercomputer) is required. Until January 2020 the University of Oslo's supercomputer Abel was used to run the Oslo CTM3. When Abel was shut down, the Oslo CTM3 migrated to Sigma2s supercomputer Saga. Some alterations had to be done after the migration to Saga, and all the job submission files had to be rewritten to work on Saga.

3.2 Oslo CTM3: Setup Used in the Simulations

This section describes the setup of the Oslo CTM3 for the simulations conducted in this thesis. First, the user options and input is described. Secondly is an explanation of how pre-industrial simulations are performed. Finally is a description of the spin-up method and how many simulations were needed to reach a state of adequate equilibrium in the model.

3.2.1 User Options and Input

When running simulations with the Oslo CTM3, user options and input has to be specified. This section explains the options and input used in this thesis.

In the *Inputfile*, the desired year, length of the simulation and the input for the initial state of the atmosphere is decided. Most of the input chosen for this thesis are the default input; however, what tracer list and emission list to use is important. All the tracers needed for the simulations are listed in the tracer list. It includes transported and non-transported species, with their names and molecular weight. For this thesis, the

tracer list *tracer_ list_ nitrate.d*, which in total contains 110 species; 96 transported and 14 non-transported, was used. The emissions list contain all emission information needed for Oslo CTM3 to run. The emission inventory used in this thesis is the Community Emissions Data System (CEDS) for historical emissions. This inventory is the Coupled Model Intercomparison Project's 6th set of historical emissions, which covers the period 1850-2014(Haslerud, 2018). The emissions lists with the CEDS emissions are named *Ltracer_ emis_ ceds17_ YEAR.inp*, where *YEAR* is replaced with the year of interest.

User options are set in the *Makefile*. Here the resolution of the model is set, and which modules and packages to include. As seen from Section 2.2.4.1, if the stratospheric routine is not included, transport from the stratosphere to the troposphere of ozone and NO_x are taken from climatology for the years 2000-2008. Ozone and NO_x are of great importance in this thesis, and the climatological values of these for the calculated period might not be very accurate, especially for pre-industrial simulations. For this reaso,n the stratosphere is included. The *Makefile* options used in this thesis are summarized in Table A.1.

As noted in Section 2.2.4.1, there are two options for methane: a fixed surface field or surface emissions. In this thesis, the fixed surface methane field has been used. Because this thesis aims to investigate the importance of photochemical reactions, running with surface emissions would lead to additional variations in the results, which are not of interest in this analysis.

3.2.2 Pre-Industrial Simulations

The pre-industrial simulations in this thesis are done for the year 1850, which is commonly used for climate analysis(e.g., Young et al., 2013; Lamarque et al., 2012; Naik et al., 2013). The tracer list used for these simulations is *Ltracer_ emis_ ceds17_ 1850.inp*. Changes made in the model to accurately simulate pre-industrial conditions are explained in this section.

As noted in Section 2.2.4.1, the methane field has to be scaled down when running pre-industrial simulations. This scaling was done by following the recipe from the Oslo CTM3 git wiki(Falk, 2020b). Here the methane value is hard-coded to 808.25 ppm to avoid the need for a very long spin-up time.

When including the stratosphere two additional changes have to be made(Tronstad, 2020). In the script *stratchem_ oslo.f90*, the input 2D data has to be taken for the year 1850. From Section 2.2.4.2 it is seen that the potential hydrogen constant has to be scaled for pre-industrial simulations as well. This is done by setting the variable *sumH2* to 5.78e-06 in *strat_ h20.f90*.

3.2.3 Model Spin-Up

When running a CTM, it is essential to let the model reach a state of statistical equilibrium under the applied forcing before starting the simulations used for producing results(Max-Planck-Institut für Meteorologie, n.d.). The time used for the model to reach this equilibrium is called the spin-up time. In this thesis, the time-slice spin-up method is used, where the model first simulates one year, before restarted for the same year but now with initial conditions taken from the first simulation. This approach is continued until adequate equilibrium is reached. The time-slice method is used because it reduces

the spin-up time by not adding additional temporal trends(Falk, 2020a).

Following is an example of how a time-slice spin-up is carried out:

1. A simulation of the year 2014 is carried out with some random initial condition. Lets call this simulation *S1*.

2. Another simulation, *S2*, of the year 2014 is carried out, now with initial conditions defined as the end results from simulation *S1*.

3. A third simulation, *S3* of the year 2014 is carried out, now with initial conditions defined as the end results from simulation *S2*.

This routine is carried out until the model reaches equilibrium, afterwards the simulations used in the analysis can start. In this thesis, the initial condition for simulation *S1*, for all scenarios, is from a simulation of the year 2001 made by Falk, 2020a.

The equilibrium is reached when

$$\frac{S_i - S_{i-1}}{S_{i-1}} < Z, \tag{3.1}$$

where S_i and S_{i-1} are values from, respectively, the i'th simulation and the previous simulation. Z is some predefined threshold value.

3.3 Experiments

This section describes the experiments conducted to examine the importance of photochemical reactions to the hydroxyl radical concentration and methane lifetime. Experiment 1 is designed to explore the importance of photodissociation of nitrogen dioxide, while Experiment 2 is designed to explore the importance of ozone photodissociation. Both experiments are simulated by using the Oslo CTM3.

3.3.1 Experiment 1

Section 2.1.4.1 explained the importance of photodissociation of nitrogen dioxide to ozone production. Because photodissociation of nitrogen dioxide is essential for ozone production, it is also vital for hydroxyl radical production(Section 2.1.5.1), and hence for methane lifetime(Section 2.1.6).

The aim of this experiment is to investigate further how important this photochemical reaction is for the concentration of ozone, hydroxyl radical and methane. This experiment is motivated by the fact that since the industrial revolution, there has been a substantial increase in gases which are mainly lost through oxidation by hydroxyl radicals(Naik et al., 2013). However, at the same time NO_x emissions have increased, leading to increased ozone production(Hoesly et al., 2018), resulting in further hydroxyl radical production. Together these two processes have offset each other when considering the hydroxyl radical, keeping its concentration relatively stable. Values for changes from pre-industrial to present-day concentrations of nitrogen dioxide, ozone and hydroxyl are found in Section 2.1.8. If the NO_x emissions had not increased during this period, or if the nitrogen dioxide

molecule had been more stable, the state of the atmosphere today would have been quite different.

This experiment considers the difference between an atmosphere where nitrogen dioxide reacts as normal and an atmosphere where it is 90% less reactive. It consists of four parts, two parts with pre-industrial conditions(1850) and two parts with modern conditions(2014). For both conditions two simulations are run, one with normal chemistry and one where the reaction rate of the photodissociation reaction with nitrogen dioxide is reduced by 90%. This setup makes it possible to compare the evolution between the two time periods for the two simulated scenarios. Table 3.1 shows a schematic description of experiment 1.

Scenario	1850	2014
Normal reaction rate (n)	$NO_2 + hv \xrightarrow{\lambda< 430nm} NO + O$	$NO_2 + hv \xrightarrow{\lambda< 430nm} NO + O$
Reduced reaction rate (rN)	$(NO_2 + hv \xrightarrow{\lambda< 430nm} NO + O)\times 0.1$	$(NO_2 + hv \xrightarrow{\lambda< 430nm} NO + O)\times 0.1$

Table 3.1: Schematic illustration of experiment 1.

Reducing the reaction rate of the photodissociation of nitrogen dioxide in the Oslo CTM3 is done by multiplying the variable *DNO2* with 0.1 in the script *pchem_ij.f90*.

3.3.2 Experiment 2

Section 2.1.4.2 showed that photodissociation of ozone to produce excited oxygen atoms is the main tropospheric ozone loss. In addition, Section 2.1.5.1 described that this same reaction is the primary source of tropospheric hydroxyl radicals, which in turn is important for the methane lifetime(Section 2.1.6).

The aim of this experiment is the same as for Experiment 1; to investigate further how important this photodissociation reaction is for the concentration of ozone, hydroxyl radical and methane. This experiment is motivated by the fact that the wavelength band needed for this reaction to occur is very narrow, only between 300-320nm. With some bad luck, this reaction would only occur in the presence of radiation with even shorter wavelengths, which does not reach the troposphere, or all radiation with wavelengths below 320nm would be stopped in the stratosphere. Such a change would profoundly affect the hydroxyl radical production in the troposphere and have severe consequences for the methane lifetime.

This experiment is build up in the same way as experiment 1. It considers the difference between an atmosphere where ozone reacts as normal and an atmosphere where photodissociation of ozone only appears 10% of the times. It consists of four parts, two parts with pre-industrial conditions(1850) and two parts with present-day conditions(2014). For both conditions, two simulations are run, one with normal chemistry and one where the reaction rate of the photodissociation of ozone is reduced by 90%. This setup makes it possible to compare the evolution between the two time periods for the two simulated scenarios. A schematic description of the experiment is seen in Table 3.2.

Scenario	1850	2014
Normal reaction rate n	$O_3 + hv \xrightarrow{300 < \lambda < 320nm} O_2 + O(^1D)$	$O_3 + hv \xrightarrow{300 < \lambda < 320nm} O_2 + O(^1D)$
Reduced reaction rate rO	$(O_3 + hv \xrightarrow{300 < \lambda < 320nm} O_2 + O(^1D)) \times 0.1$	$(O_3 + hv \xrightarrow{300 < \lambda < 320nm} O_2 + O(^1D)) \times 0.1$

Table 3.2: Schematic illustration of experiment 2.

Reducing the reaction rate of the photodissociation of ozone in the Oslo CTM3 is done by multiplying the variable *DBO3* with 0.1 in the script *pchem_ ij.f90*.

3.3.3 Hypotheses

This section presents some hypotheses made to Experiment 1 and Experiment 2 in the search for answers to the research questions(Section 1.1). Some of the hypotheses are the same for both experiments, while others are not. The hypotheses' which are only valid for one of the two experiments are marked with bold fonts.

1. The difference between the scenarios are less prominent for pre-industrial conditions than for present-day conditions, as the concentrations of nitrogen dioxide, ozone and methane were lower in 1850.

2. The difference in global distribution between the scenarios are more prominent in lower latitudes and regions with high NO_x emissions, since the controlling effects are the abundance of NO_x and solar insolation.

3. **Experiment 1**: Ozone concentrations are considerably smaller in the reduced reaction rate scenario, but retain the same trend as in the normal reaction rate scenario. This is because the production through photodissociation of NO_x is turned down by a constant percentage, making the source of ozone lower but still increasing with higher NO_x concentrations.

4. **Experiment 2**: Ozone concentrations are considerably higher in the reduced reaction rate scenario, but retain the same trend as in the normal reaction rate scenario. This is because the only change is that the loss through photodissociation is turned down by a constant percentage, making the sink of ozone lower.

5. **Experiment 1:** Nitrogen dioxide concentrations are elevated, and the ratio between nitrogen dioxide and nitrogen monoxide ratio is shifted towards nitrogen dioxide. This is because the rapid cycling between nitrogen dioxide and nitrogen monoxide would slow down where nitrogen dioxide are photodissociated, producing nitrogen monoxide.

6. **Experiment 2:** Nitrogen dioxide concentrations are lower because the ozone concentration is elevated.

7. Hydroxyl radical concentrations increase less from 1850 to 2014 in the reduced reaction rate scenarios compared to the normal, because its sources decrease and its sinks increase.

8. The increase in methane concentration is greater between 1850 and 2014 for the reduced reaction rate scenarios than for the normal reaction rate scenario, because of lower hydroxyl radical concentrations and no change in methane emissions.

3.4 Preprocessing of Data

The output of the Oslo CTM3 is numerous large netCDF files on another format than desired, so it is useful to preprocess the data before analyzing it. Some of this preprocessing has been done by using the climate data operator(CDO), a software which has collected operators for standard processing of climate and forecast model data(Schulzweida et al., 2006). This has been used to:

1. Convert from mass mixing ratio to volume mixing ratio(explained in Section 3.4.1)

2. Calculate zonal mean

3. Concatenate data

In addition the tropopause has been defined(explained in Section 3.4.2.)

3.4.1 Unit Conversion

The output of the Oslo CTM3 is given in mass mixing ratio(kg/kg), while the desired unit for this analysis is volume mixing ratio(mol/mol). The following equation does the conversion from mass mixing ratio(mmr) to volume mixing ratio(vmr)

$$vmr = \frac{m_t}{m_a}\frac{M_a}{M_t}, \tag{3.2}$$

where m_t is the mass of the specific tracer, m_a is the mass of air, M_a is the molecular weight of air and M_t the molecular weight of the tracer. The molecular masses are fixed, while the masses are spatially variable. The molecular weights used can be seen in Table 3.3, while the masses are taken from the output of the simulations.

3.4.2 Defining the Tropopause

The tropopause is the boundary between the troposphere and the stratosphere. Where in the atmosphere the tropopause can be found by looking at the lapse rate or potential vorticity units(Wallace et al., 2006). However, for simplicity, the climatological tropopause is used to isolate the troposphere in this thesis.

Inspiration has been drawn from the results of Graversen et al. (2014) when defining the tropopause. Their results can be seen in Figure 3.1, and have been found by using a slab-ocean mode in the Community Climate System Model, version 4(CCSM4). The climatological field are from two 70-year experiments between year 21 and 70, one with

Molecule	Molecular Weight (g/mol)
CH_4	16.042
O_3	47.9982
OH	17.01
NO_2	46.0055
NO	30.0061
Air	28.9644

Table 3.3: Molecular masses of chemical species considered in this thesis.

a carbon dioxide concentration of 284.7ppm(named $1 \times CO_2$, illustrating pre-industrial conditions) and one with a carbon dioxide concentration of 569.4ppm(named $2 \times CO_2$).

Figure 3.2 shows how the troposphere is defined in this thesis. This definition is made by the inspiration from Figure 3.1 and the tropospheric layers available in the Oslo CTM3. The method is an approximation and will lead to some inaccuracies in the results, as the tropopause height will vary through the simulation and the different scenarios. In 1850 the carbon monoxide concentration was 280ppm(Goll et al., 2014), while in 2014 it was 397.2ppm(Kennedy, 2015). Even though the 1850 carbon monoxide concentration is slightly lower, and the 2014 concentration higher, the tropopause from the $1 \times CO_2$ experiment is used for all simulations.

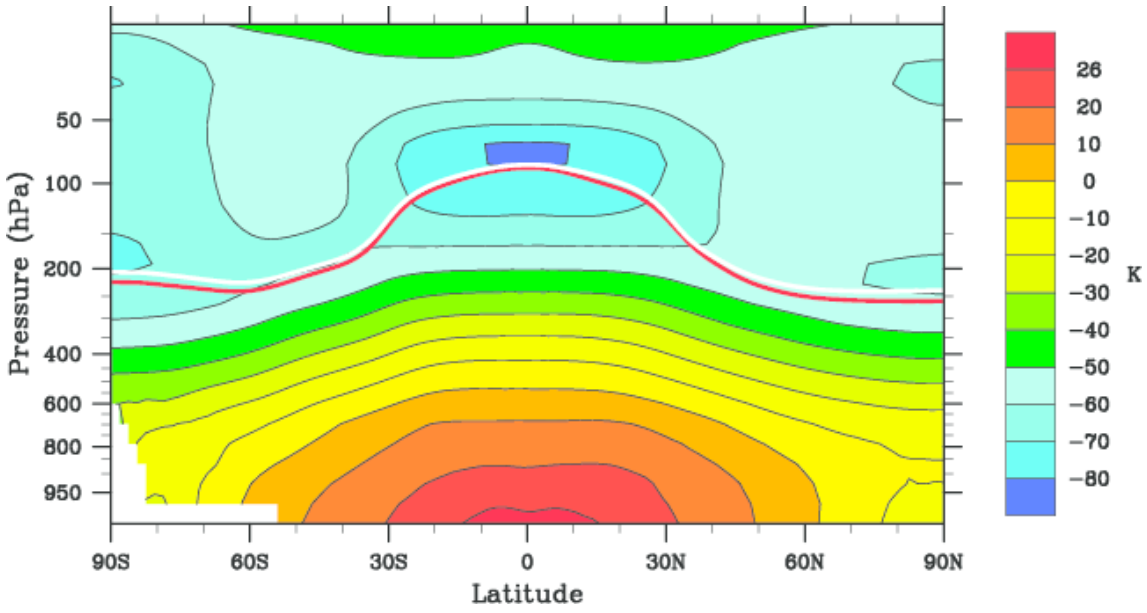

Figure 3.1: Zonal and annual mean climatological tropopause height as a function of latitude. The red line symbolizes the tropopause in the $1 \times CO_2$ experiment, while the white line the $2 \times CO_2$ experiment. Image taken from Graversen et al., 2014.

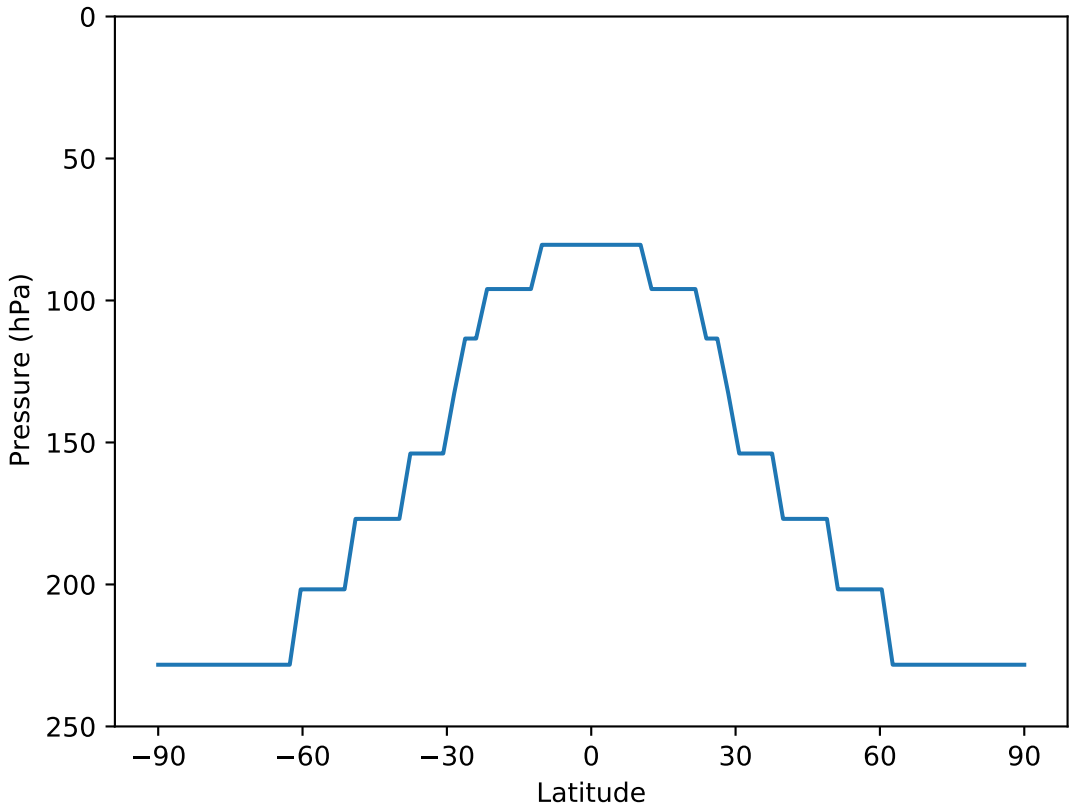

Figure 3.2: Defined Climatological tropopause used in this thesis, inspired by Figure 3.1, made by using the tropospheric pressure levels in the Oslo CTM3 output. Note that the pressure level here start at 250hPa.

3.5 Analysis

This section describes the methods used to analyze the preprocessed Oslo CTM3 output from the conducted simulations, and where the methane lifetimes are found. First, the spin-up analysis is presented. Second is an explanation of the methane lifetime before the methods used for comparing the results from the different scenarios are presented. Finally, how infinite values are handled is explained.

3.5.1 Spin-Up Analysis

Whether the model is in equilibrium or not, is in this thesis decided by the equation

$$\frac{S_i - S_{i-1}}{S_{i-1}} < 1‰. \tag{3.3}$$

This inequality is recognized as the Equation 3.1, explained in Section 3.2.3, with Z set to 1‰. The inequalities are identified by

$$\text{Year+scenario} \quad S(i-1) - Si,$$

where *Year* is either 1850 or 2014, and the scenario is either the normal(n), reduced reaction rate of nitrogen dioxide(rN) or ozone rO photodissociation. Si is the i'th simulation for the scenario and *S(i-1)* the previous simulation.

Only the tropospheric values are of interest, so the equilibrium is calculated only for the tropospheric layers in the model(the uppermost level is taken as 34 for all latitudes). The model is decided to be in adequate equilibrium when 90% of the simulated tropospheric values are below the threshold. Longlived species takes longer to reach equilibrium(Falk, 2020a). Methane being the species of interest with the longest lifetime it is the one deciding the number of spin-up simulations needed.

The troposphere is divided into three vertical layers, illustrating the lower, middle and upper troposphere. Because the surface methane field is fixed in the simulations, equilibrium is reached quickly in the lowermost layers. In the upper troposphere, methane concentrations are lower, and small changes result in significant percentage change. Therefore it takes longer for the model to reach equilibrium in the uppermost tropospheric layers.

Table 3.4 shows the percentage of tropospheric methane values under 1‰after going through Equation 3.3 for the spin-up simulations run for this thesis. From the table, it is evident that the model reaches equilibrium(90% of the values fulfils the inequality 3.3) during the third spin-up simulation. The only exceptions are layer 20-34 in *2014rN S2-S3* and *2014rO S2-S3*, however, it is close, so another spin-up simulation is not conducted.

Simulations	Lower	Middle	Upper
2014n S1-S2	99.6	96.4	69.7
2014n S2-S3	100.0	100.0	91.5
2014rN S1-S2	99.3	89.3	69.2
2014rN S2-S3	100.0	100.0	89.4
2014rO S1-S2	99.5	89.7	65.3
2014rO S2-S3	100.0	99.9	87.7
1850n S1-S2	98.9	89.5	46.4
1850n S2-S3	100.0	100.0	95.4
1850rN S1-S2	98.8	90.0	49.5
1850rN S2-S3	100.0	100.0	95.5
1850rO S1-S2	99.0	90.2	48.1
1850rO S2-S3	100.0	100.0	95.6

Table 3.4: Percentage of methane values, for two consecutive simulations, achieving the equilibrium requirement set for this thesis(Equation 3.3), divided in three vertical tropospheric layers: Lower(Layer 0-1), Middle(Layer2-29) and Upper(Layer30-34). The simulations denoted by n are the ones with normal reaction rates, rN and rO the ones with reduced reaction rate for, respectively, photodissociation of nitrogen dioxide and ozone. S1 is the first simulated year, S2 the second and S3 the third.

3.5.2 Methane Lifetime

In this thesis, it is methane's lifetime to oxidation by the hydroxyl radical which are of interest. The Oslo CTM3 output two methane lifetimes to oxidation by the hydroxyl radical; SFC-LTOP and Lawrence. In SFC-LTOP, the lifetime is calculated as the mean from the surface to the uppermost layer in the model, while the Lawrence method is a kernel method to correct for the temperature-dependent oxidation, valid below the climatological tropopause(Falk, 2020a).

3.5.3 Comparisons

To answer the research questions in this thesis, many comparisons have to be executed, between concentrations in 1850 and 2014 and between the different scenarios. These are presented either as a change in concentration or per cent change. Comparing two simulations, the difference in concentration is calculated simply by subtraction

$$x - y, \tag{3.4}$$

while the percentage change is calculated as

$$\left(\frac{x-y}{y}\right) \times 100. \tag{3.5}$$

Here x and y represents the two scenarios compared.

When comparing the difference between four simulations, for example comparing the change between 1850 and 2014 in one scenario to another, absolute values are used, in case of a negative difference in one or both scenarios. For difference given in concentration, this is done as

$$|x - y| - |a - b|, \tag{3.6}$$

while the difference in percentage as

$$\left(\frac{|x-y| - |a-b|}{|a-b|}\right) \times 100, \tag{3.7}$$

where x,y,a and b represents the four scenarios compared.

3.5.4 Handling Infinite Values

During the analysis, infinite values were encountered for some of the species. These values became a problem when finding the mean value over any dimension. Additionally, this was not realistic values, and they were replaced with *Not a Number*(NaN). When later calculating the mean values, all NaN values were ignored not to alter the results. This method might lead to error in the results, as not all values are correctly represented.

Chapter 4

Results

This chapter presents the results of the simulations and analysis made to answer the research questions. First presented is the difference between scenarios for present-day(2014) compared to pre-industrial(1850). All following results consider the difference in change between 1850 and 2014, for example, ozone concentration change between 1850 to 2014 in the normal scenario. Secondly, the spatial distribution is examined before the vertical distribution is considered. Then results for the methane lifetime are presented. Finally, the two reduced reaction rate scenarios are compared.

In the results, abbreviations are used to identify the scenarios. The normal scenario is identified by n, the scenario with reduced photodissociation of nitrogen dioxide by rN and the scenario with reduced photodissociation of ozone by rO. For example *2014rN-2014n* would mean the 2014 reduced photodissociation of nitrogen dioxide scenario subtracted the 2014 normal scenario.

In some of the sections, not all species are represented. This will be noted and explained in the respective sections.

4.1 Is There a Difference Between the Scenarios?

The first thing to investigate is whether or not there is a difference between the normal scenario and the ones with reduced reaction rates. This difference is found by subtracting the values of the normal scenario from the reduced reaction rate scenarios for the same year— for example, *2014rN-2014n*. The second step is to examine if the contrast is more significant in 2014 than in 1850(first hypothesis from Section 3.3.3). This contrast is examined by subtracting the difference between two 2014 scenarios from the parallel 1850 scenarios, for example, $|$*2014rN-2014n*$|$-$|$*1850rN-1850n*$|$, where the absolute values are used to ensure that the result is the actual difference(in case of negative values). This section presents the results found through that analysis.

Figure 4.1 shows the difference in total tropospheric ozone concentrations between the normal and the reduced reaction rate scenarios. In the rN scenarios, the ozone concentration is lower than in the normal scenario, indicated by the negative difference(4.1a and 4.1c). The annual pattern is similar for 2014 and 1850, with the largest difference during northern hemisphere spring. However, the difference is larger in 2014 than 1850, which is further confirmed by 4.1e where it is also seen that the difference is most prominent during the high difference season. When looking at the rO scenarios, the ozone concentration

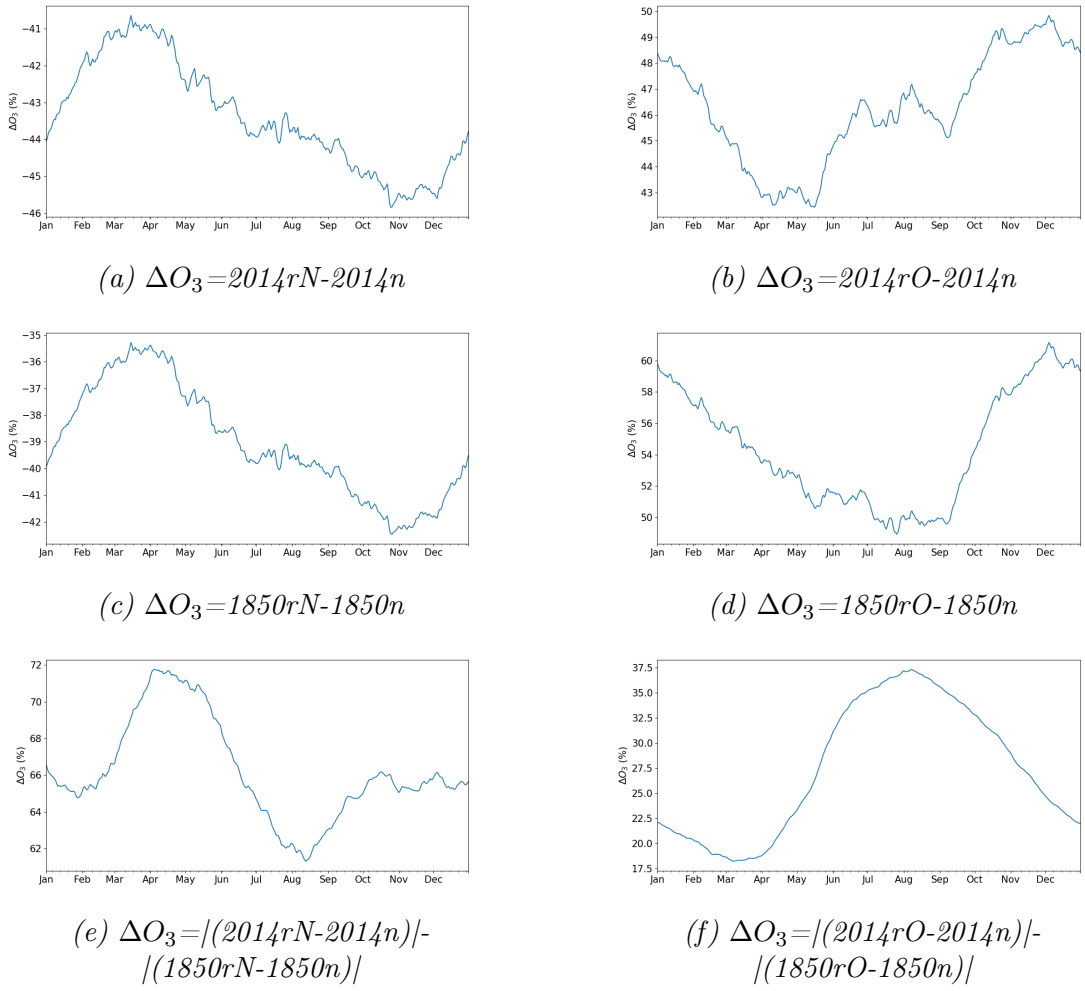

(a) ΔO_3*=2014rN-2014n*

(b) ΔO_3*=2014rO-2014n*

(c) ΔO_3*=1850rN-1850n*

(d) ΔO_3*=1850rO-1850n*

(e) ΔO_3*=|(2014rN-2014n)|-|(1850rN-1850n)|*

(f) ΔO_3*=|(2014rO-2014n)|-|(1850rO-1850n)|*

Figure 4.1: Difference in total ozone concentration. The figures show the results made by summing over latitude, longitude and vertical level and taking the mean over each day. Figures (e) and (f) are the results from subtracting, respectively, the results (a)-(c) and (b)-(d). Note that the the results in (e) and (f) are found by using absolute values.

is higher than in the normal scenario, indicated by the positive difference (in 4.1b and 4.1d). In both 2014 and 1850 the most prominent difference between rO and n is during northern hemisphere winter. From Figure 4.1f it is seen that the difference is greater in 2014 than in 1850, with the largest difference during northern hemisphere summer to early autumn.

Figure 4.2 shows the difference in total tropospheric hydroxyl radical concentration between the normal scenario and the reduced reaction rate scenarios. The differences between the reduced reaction rate scenarios and the normal(4.2a-4.2d) have a similar annual pattern, with the largest differences during northern hemisphere winter and early spring. January of 1850 is the exception, where the difference is low. There is generally lower hydroxyl radical concentration in both the reduced reaction rate scenarios compared to the normal, indicated by the negative values, with the only exception being some periods during June-October in the rO 2014 scenario. Considering the difference between 2014 and 1850, seen in 4.2e and 4.2f, the difference is greater in 2014 and most prominent

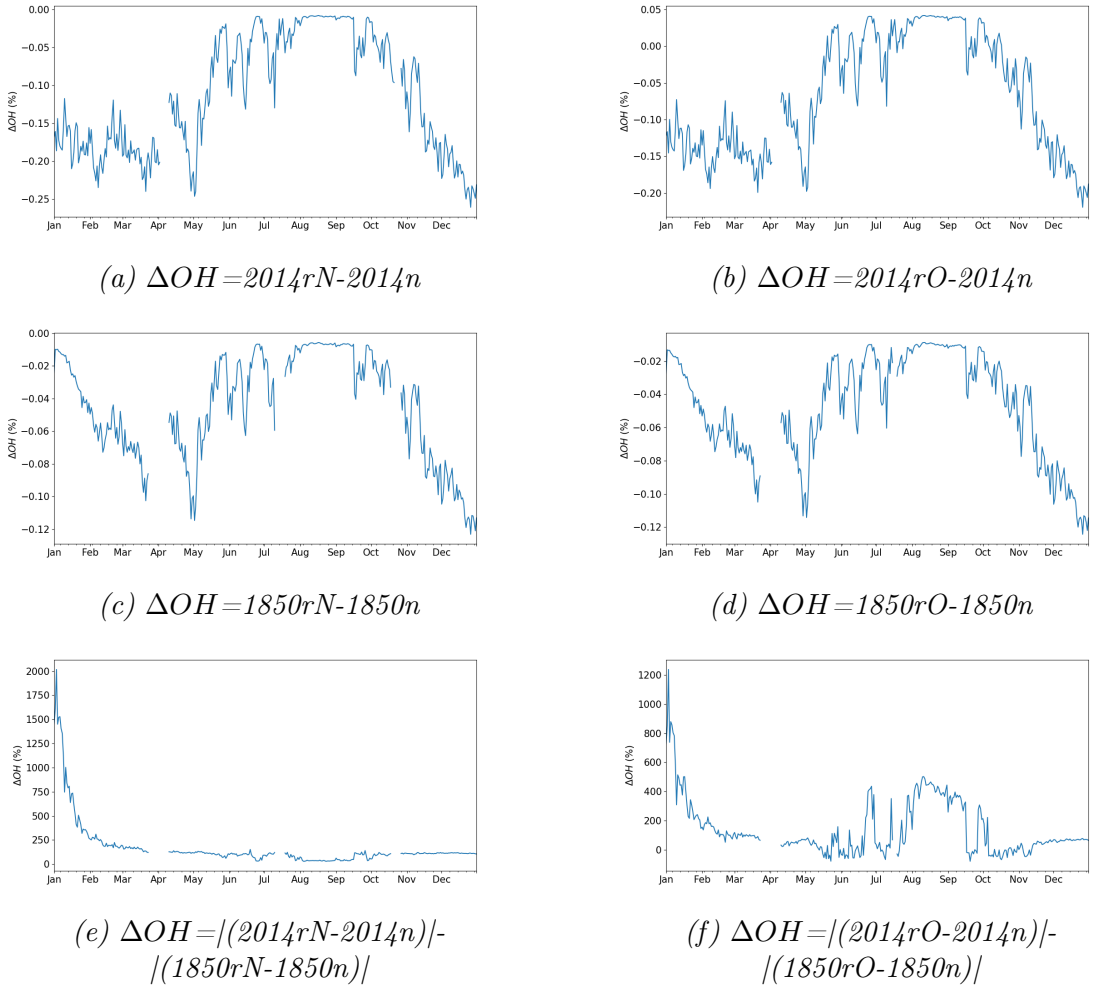

(a) ΔOH =2014rN-2014n

(b) ΔOH =2014rO-2014n

(c) ΔOH =1850rN-1850n

(d) ΔOH =1850rO-1850n

(e) ΔOH =|(2014rN-2014n)|-|(1850rN-1850n)|

(f) ΔOH =|(2014rO-2014n)|-|(1850rO-1850n)|

Figure 4.2: Difference in total hydroxyl radical concentration. The figures show the results made by summing over latitude, longitude and vertical level and taking the mean over each day. Figures (e) and (f) are the results from subtracting, respectively, the results (a)-(c) and (b)-(d). Note that the the results in (e) and (f) are found by using absolute values.

at the start of the year. For the *rO* scenario, there are also elevated differences during northern hemisphere summer and early autumn.

Figure 4.3 shows the difference in total tropospheric methane concentration between the reduced reaction rate scenarios and the normal. The difference between the *rN* and *n* scenarios, seen in 4.3a and 4.3c, shows that the methane concentration is higher in the *rN* than the *n* scenario. In 2014, the difference is largest during northern hemisphere late spring to early autumn, while in 1850 the difference in least prominent during January, and quite stable the rest of the year. The difference is larger in 2014, confirmed by the results in 4.3e, and most noticeable early in the year. Comparing the *rO* scenario to the normal one, it is seen that the patterns are very similar to those of the *rN* and *n* scenario. The only noticeable inequality is somewhat higher differences in 2014, 4.3b.

Figure 4.4 shows the difference in total tropospheric nitrogen dioxide concentrations between the reduced reaction rate scenarios and the normal. In 4.4a and 4.4c, it is seen

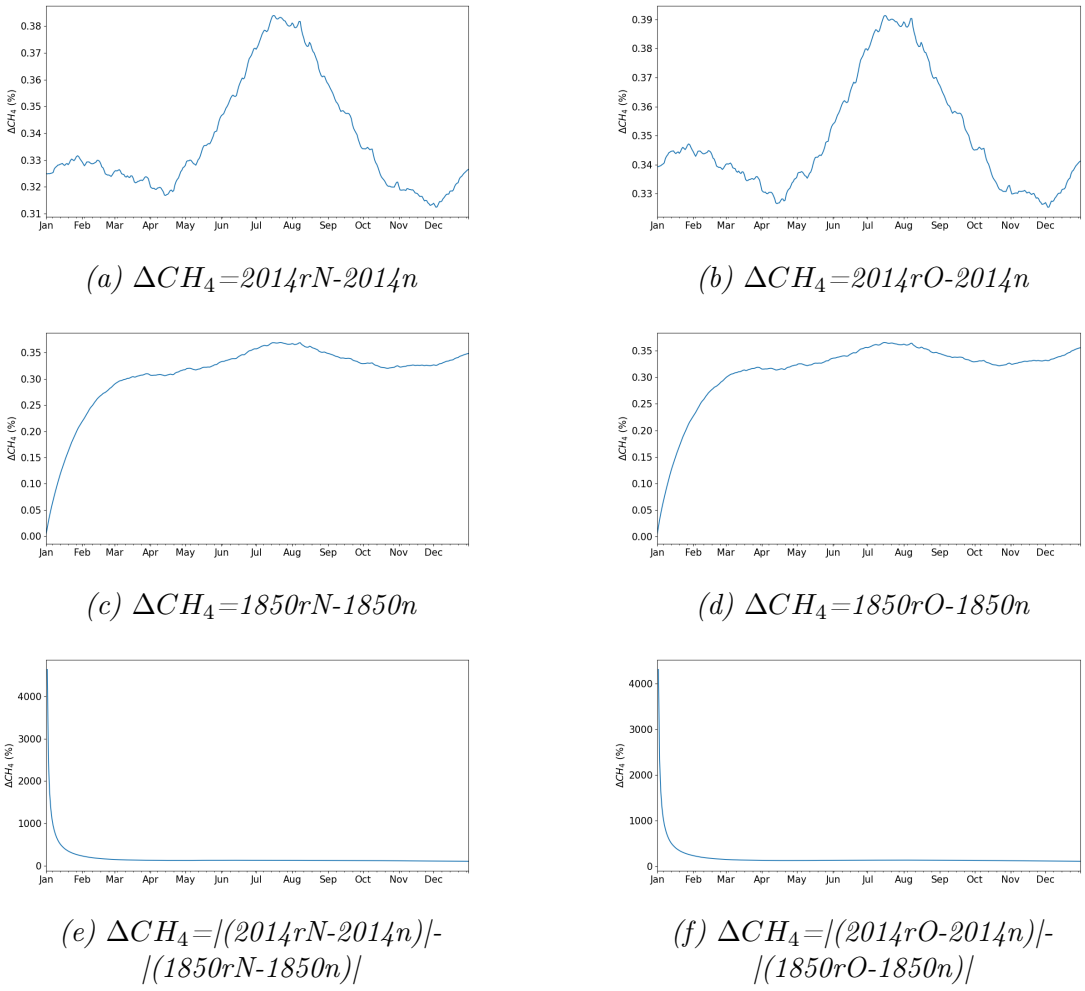

(a) ΔCH_4*=2014rN-2014n*

(b) ΔCH_4*=2014rO-2014n*

(c) ΔCH_4*=1850rN-1850n*

(d) ΔCH_4*=1850rO-1850n*

(e) ΔCH_4*=|(2014rN-2014n)|-|(1850rN-1850n)|*

(f) ΔCH_4*=|(2014rO-2014n)|-|(1850rO-1850n)|*

Figure 4.3: Difference in total methane concentration. The figures show the results made by summing over latitude, longitude and vertical level and taking the mean over each day. Figures (e) and (f) are the results from subtracting, respectively, the results (a)-(c) and (b)-(d). Note that the the results in (e) and (f) are found by using absolute values.

that the nitrogen dioxide concentration is higher in the rN than the n scenario. In 2014, the peak of the difference is during northern hemisphere late autumn to early spring, while in 1850 during summer and autumn. The difference is greater in 2014, confirmed by 4.4e, and the pattern here follows the one seen for 2014(4.4a). Considering the difference between the rO and n scenarios, the results are not as one sided. In 2014, the nitrogen dioxide concentration is higher in the rO scenario from March to October and lower the rest of the year. A similar pattern is seen 1850, except that the period with positive difference in nitrogen dioxide concentrations are narrower, occurring only during July to September. The difference between the rO and n scenarios is larger in 2014 than in 1850, with peaks during the period where the nitrogen dioxide concentration is higher in the rO scenario.

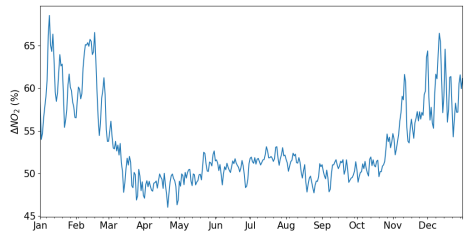

(a) ΔNO_2*=2014rN-2014n*

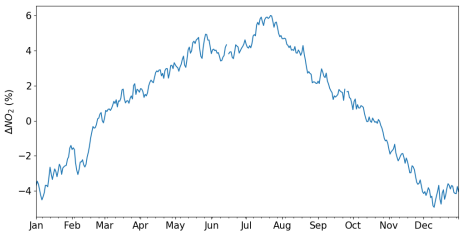

(b) $\Delta NO2$*=2014rO-2014n*

(c) ΔNO_2*=1850rN-1850n*

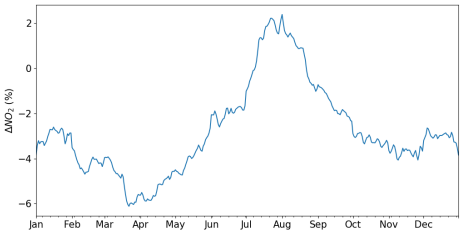

(d) ΔNO_2*=1850rO-1850n*

(e) ΔNO_2*=|(2014rN-2014n)|-|(1850rN-1850n)|*

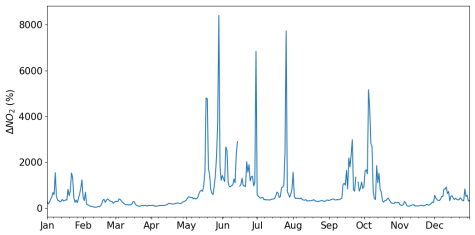

(f) ΔNO_2*=|(2014rO-2014n)|-|(1850rO-1850n)|*

Figure 4.4: Difference in total nitrogen dioxide concentration. The figures show the results made by summing over latitude, longitude and vertical level and taking the mean over each day. Figures (e) and (f) are the results from subtracting, respectively, the results (a)-(c) and (b)-(d). Note that the the results in (e) and (f) are found by using absolute values.

4.2 Global Distribution

The second thing interesting to look into is the global distribution. Hypotheses two in Section 3.3.3 is that the difference between the reduced reaction rate scenarios and the normal are more prominent in lower latitudes and regions with high NO_x emissions. This spatial difference indicates that global distribution is worth consideration and will be investigated by first looking at the time mean total latitudinal difference, then the total tropospheric column difference. This section presents the results of this analysis. Results for the hydroxyl radical and results for nitrogen dioxide when considering total column concentrations are not included due to problems in the analysis.

Figure 4.5 shows the mean latitudinal ozone concentration change between 1850 and 2014 for the reduced reaction rate scenarios and the normal. As seen from 4.5a - 4.5c the ozone concentrations are higher in 2014 than in 1850. This difference is more prominent

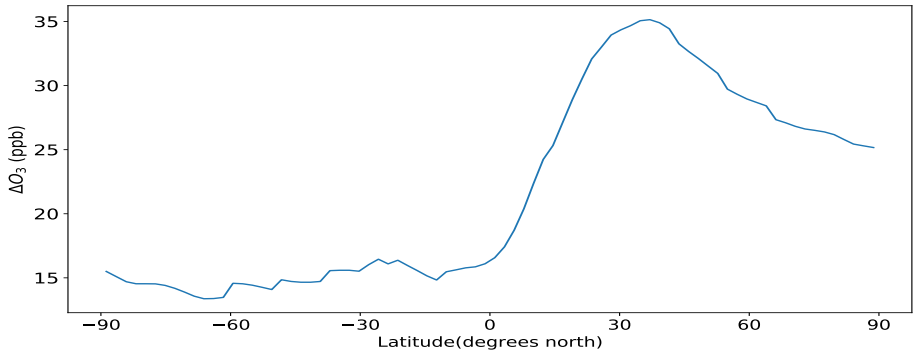

(a) ΔO_3*=2014n-1850n*

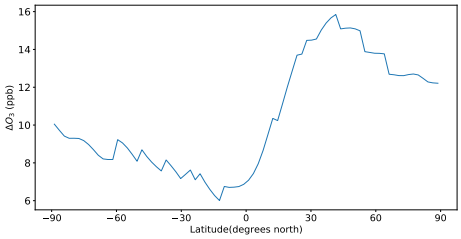

(b) ΔO_3*=2014rN-1850rN*

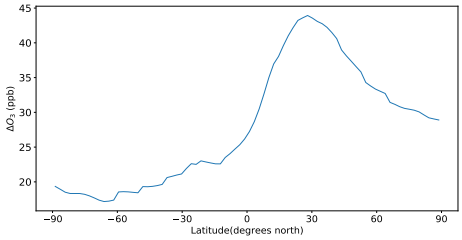

(c) ΔO_3*=2014rO-1850rN*

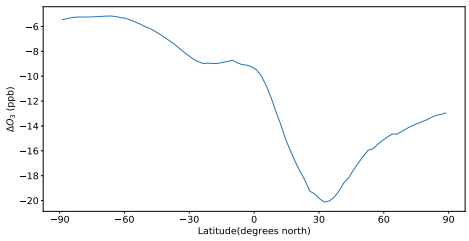

(d) ΔO_3*=|(2014rN-1850rN)|-|(2014n-1850n)|*

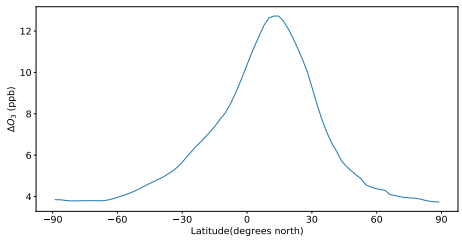

(e) ΔO_3*=|(2014rO-1850rO)|-|(2014n-1850n)|*

Figure 4.5: Latitudinal difference in ozone concentration. The figures show the results made by taking the mean over longitude, vertical level and time. The change between 1850 and 2014 for the normal scenario is shown in (a), while (b) and (c) show the same change, respectively, for the rN and rO scenarios. Figures (d) and (e) are the results from subtracting, respectively, the results (b)-(a) and (c)-(a).

in the northern than in the southern hemisphere, for all scenarios, with a peak around 30N. The difference in change from 1850 and 2014 between the *rN* and the *n* scenarios is seen in 4.5d. This difference shows that the ozone concentration is lower in the *rN* scenario and that it is most prominent at latitudes where the change between 1850 to 2014 is largest. Figure 4.5e shows the difference between the *rO* and *n* scenarios, where the change in ozone concentrations between 1850 and 2014 is higher in the former. In contrast to the other results in Figure 4.5, the peak difference is closer to the equator.

The change in latitudinal hydroxyl radical concentration from 1850 to 2014 is seen in Figure 4.6. From 4.6a-4.6c it is seen that the pattern of change is similar for all the scenarios, with the most prominent differences at high latitudes. From about 80S-80N, the

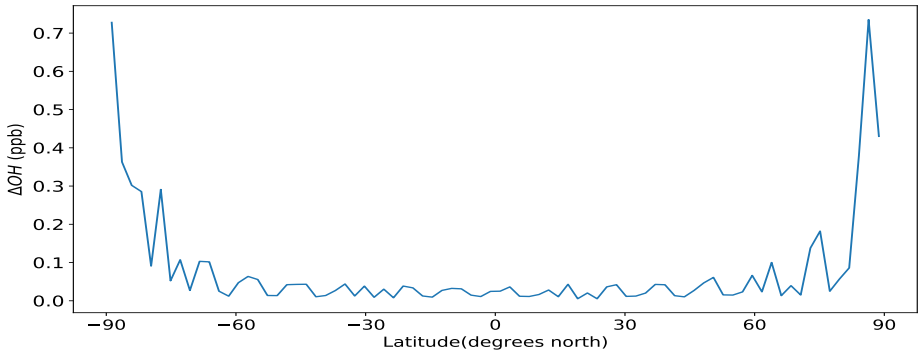

(a) ΔOH =2014n-1850n

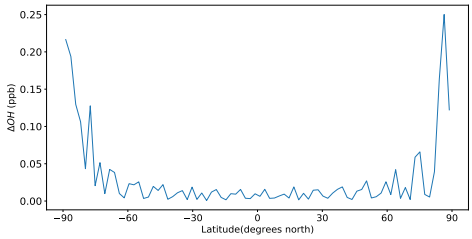

(b) ΔOH =2014rN-1850rN

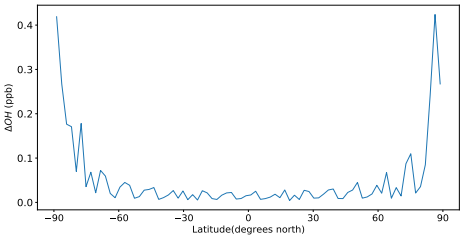

(c) ΔOH =2014rO-1850rN

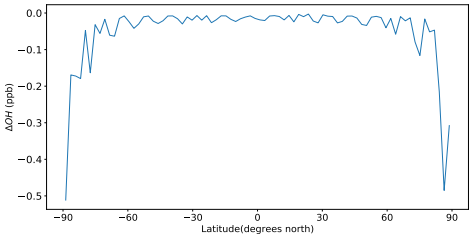

(d) ΔOH =|(2014rN-1850rN)|-|(2014n-1850n)|

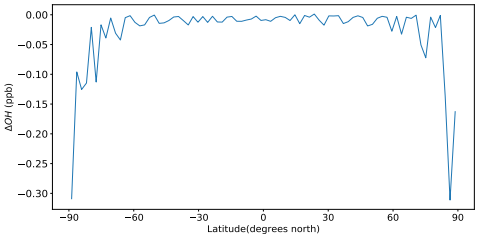

(e) ΔOH =|(2014rO-1850rO)|-|(2014n-1850n)|

Figure 4.6: Latitudinal difference in hydroxyl radical concentration. The figures show the results made by taking the mean over longitude, vertical level and time. The change between 1850 and 2014 for the normal scenario is shown in (a), while (b) and (c) show the same change, respectively, for the rN and rO scenarios. Figures (d) and (e) are the results from subtracting, respectively, the results (b)-(a) and (c)-(a).

change is close to zero. The difference between the reduced reaction rate scenarios and the normal, seen in 4.6d and 4.6e, shows that there are lower hydroxyl radical concentrations in the reduced reaction rate scenarios, indicated by negative values. Also here the same pattern is seen, with little change between about 80S to 80N.

Figure 4.7 shows the mean latitudinal methane concentration between 1850 and 2014 for the normal and the reduced reaction rate scenarios. The results in 4.7a - 4.7c look very similar, with difference increasing from 90S to 90N. Considering the difference between 1850 to 2014, seen in 4.7d and 4.7e, the difference is largest at low latitudes and is similar in both comparisons.

Figure 4.8 shows the mean latitudinal nitrogen dioxide concentration difference be-

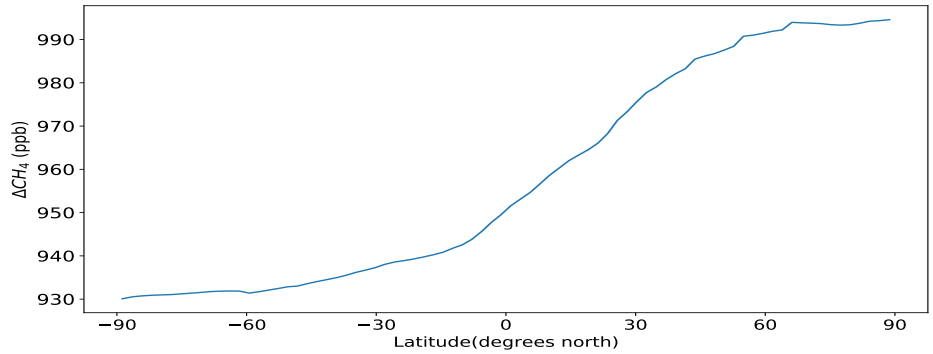

(a) ΔCH4=2014n-1850n

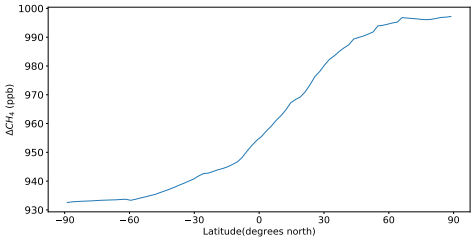

(b) ΔCH_4=2014rN-1850rN

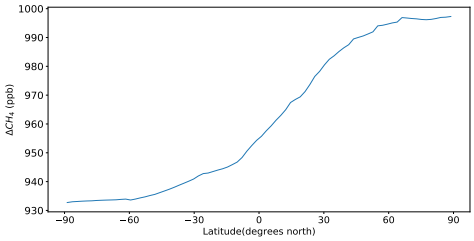

(c) ΔCH_4=2014rO-1850rO

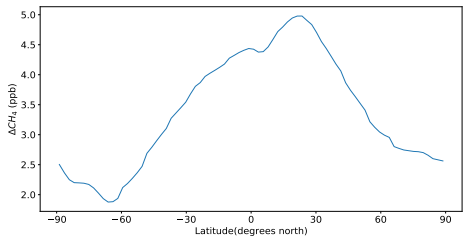

(d) ΔCH_4=/(2014rN-1850rN)/-/(2014n-1850n)/

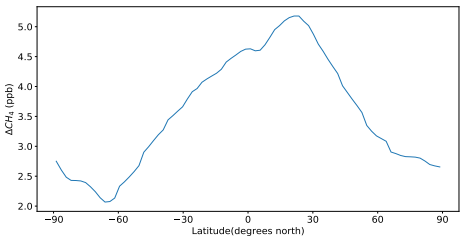

(e) ΔCH_4=/(2014rO-1850rO)/-/(2014n-1850n)/

Figure 4.7: Latitudinal difference in methane concentration. The figures show the results made by taking the mean over longitude, vertical level and time. The change between 1850 and 2014 for the normal scenario is shown in (a), while (b) and (c) show the same change, respectively, for the rN and rO scenarios. Figures (d) and (e) are the results from subtracting, respectively, the results (b)-(a) and (c)-(a).

tween 1850 and 2014 for the reduced reaction rate scenarios and the normal. The pattern of change, seen in 4.8a-4.8c, is similar for all three scenarios, with the largest difference occurring in northern mid latitudes. Considering the difference in change between the *rN* scenarios and the normal, Figure 4.8d, there is generally a greater change in the *rN* scenario than the normal. There is, however, little difference between the two scenarios from 90-60S, and an even somewhat negative difference(less nitrogen dioxide in the *rN* than the *n* scenario) around 60N. Figure 4.8e shows the difference in change between the *rO* and *n* scenarios, where little difference is seen between 90S to about 40S, a positive difference around 30S and negative difference from about 30S to the equator.

Figure 4.9 shows the change in total tropospheric column ozone concentration between

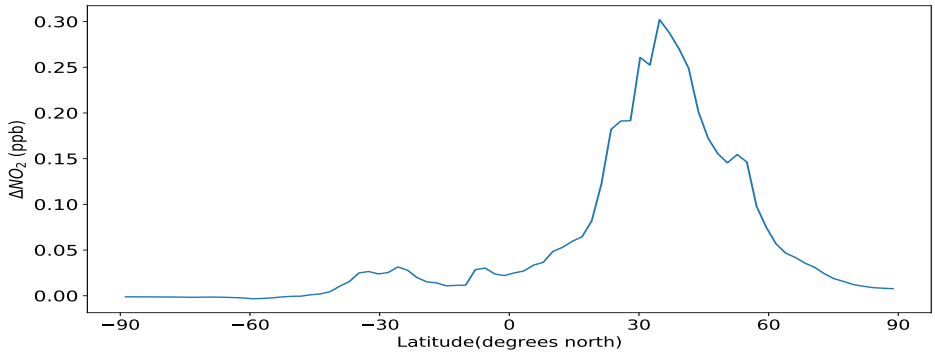

(a) ΔNO_2=2014n-1850n

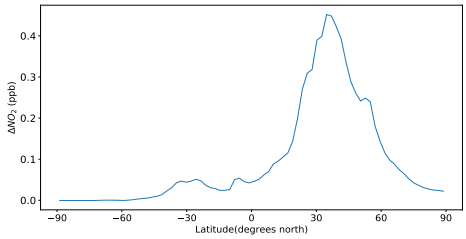

(b) ΔNO_2=2014rN-1850rN

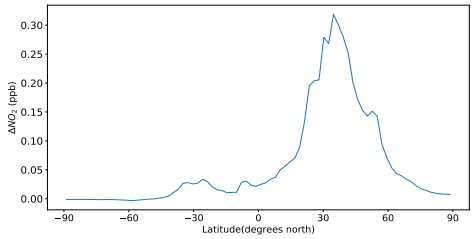

(c) ΔNO_2=2014rO-1850rO

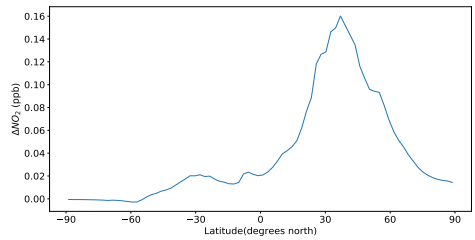

(d) ΔNO_2=|(2014rN-1850rN)|-|(2014n-1850n)|

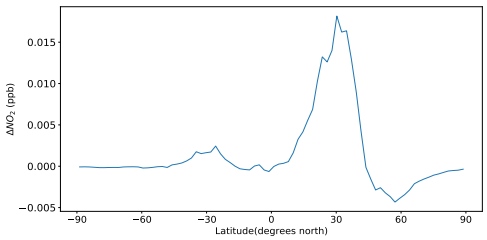

(e) ΔNO_2=|(2014rO-1850rO)|-|(2014n-1850n)|

Figure 4.8: Latitudinal difference in nitrogen dioxide concentration. The figures show the results made by taking the mean over longitude, vertical level and time. The change between 1850 and 2014 for the normal scenario is shown in (a), while (b) and (c) show the same change, respectively, for the rN and rO scenarios. Figures (d) and (e) are the results from subtracting, respectively, the results (b)-(a) and (c)-(a).

1850 and 2014 for the normal scenario and the reduced reaction rate scenarios. The greatest change, for all scenarios, is in the northern hemisphere, especially over southern Asia. Looking at the difference between the change in the *rN* and *n* scenarios, seen in 4.9d, a lower change is seen for the *rN* scenario than the normal, indicated by negative values. The largest difference is seen in the northern hemisphere, peaking over India and southeast China. Considering the difference between the change in the *rO* and *n* scenarios, Figure 4.9e, the greater change is occurring in *rO*, indicated by the positive values. The largest difference is seen close to the equator in the northern hemisphere, with a peak in the Pacific Ocean, while the least difference is found over China around Beijing.

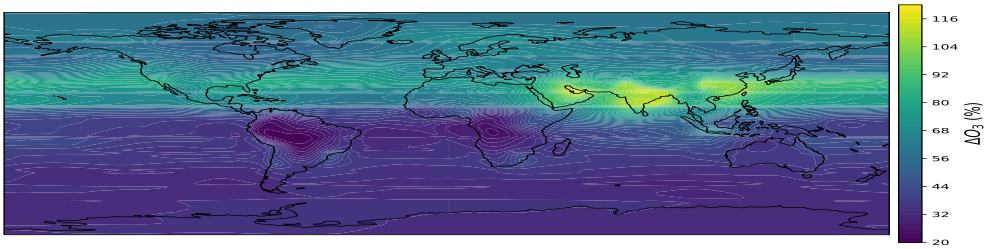

(a) ΔO_3*=2014n-1850n*

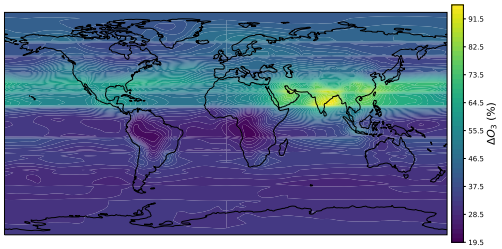

(b) ΔO_3*=2014rN-1850rN*

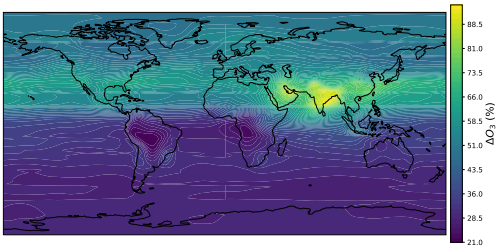

(c) ΔO_3*=2014rO-1850rO*

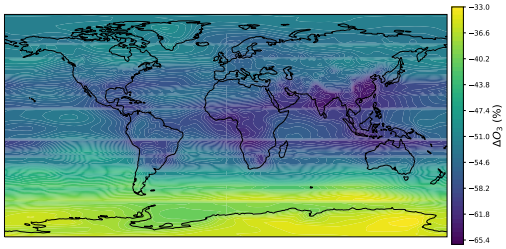

(d) ΔO_3*=|(2014rN-1850rN)|-*
|(2014n-1850n)|

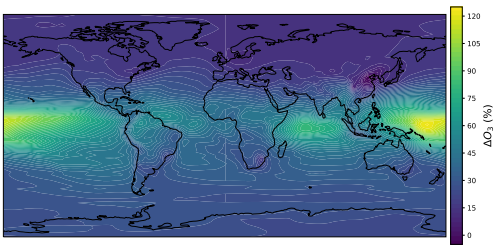

(e) ΔO_3*=|(2014rO-1850rO)|-*
|(2014n-1850n)|

Figure 4.9: Total tropospheric column ozone concentration. The figures show the results made by summing over the tropospheric levels and taking the mean over time. The change between 1850 and 2014 for the normal scenario is shown in (a), while (b) and (c) show the same change, respectively, for the rN and rO scenarios. The difference in change between the rN and rO scenarios and the normal is seen, respectively, in (d) and (e). Note that each part of the figure has its own colour bar, and that these differ.

The change in total tropospheric methane column between 1850 and 2014 for the normal and the reduced reaction rate scenarios is shown in Figure 4.10. The pattern of the change is similar among the three scenarios, except that the values are slightly higher in the reduced reaction scenarios. 4.10d-4.10e confirms this slightly higher change in methane in the reduced reaction rate scenarios as compared with the normal. The pattern of the difference between the scenarios is similar, with the least change at southern hemisphere high latitudes and the most noticeable difference in low northern latitudes, peaking over southern Asia.

Figure 4.11 shows the change in total tropospheric nitrogen dioxide column concentra-

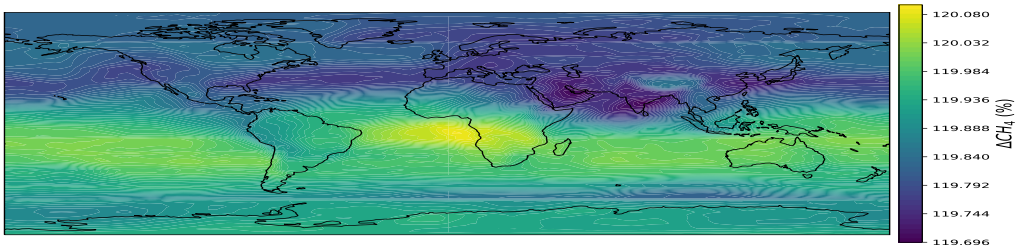

(a) ΔCH_4*=2014n-1850n*

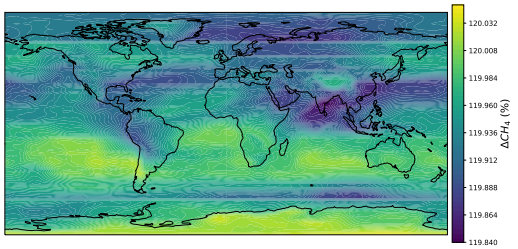

(b) ΔCH_4*=2014rN-1850rN*

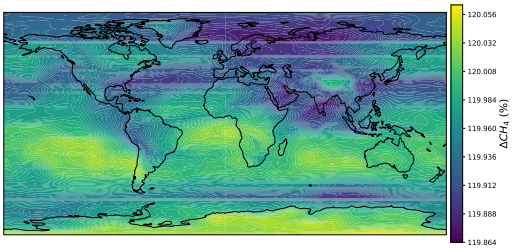

(c) ΔCH_4*=2014rO-1850rO*

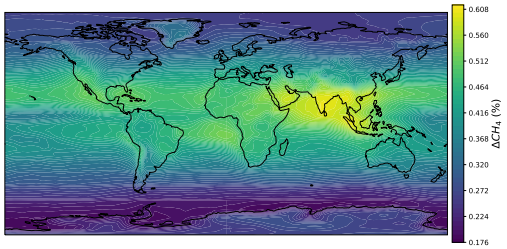

(d) ΔCH_4*=|(2014rN-1850rN)|-|(2014n-1850n)|*

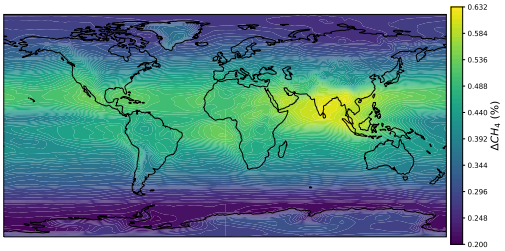

(e) ΔCH_4*=|(2014rO-1850rO)|-|(2014n-1850n)|*

Figure 4.10: Total tropospheric column methane concentration. The figures show the results made by summing over the tropospheric levels and taking the mean over time. The change between 1850 and 2014 for the normal scenario is shown in (a), while (b) and (c) show the same change, respectively, for the rN and rO scenarios. The difference in change between the rN and rO scenarios and the normal is seen, respectively, in (d) and (e). Note that each part of the figure has its own colour bar, and that these differ.

tion between 1850 and 2014 in the normal and the *rN* scenario and the difference between them. From 4.11a and 4.11b it is seen that the change between 1850 and 2014 over most of the world is close to zero. There are, however, some places where the change is greater than others, and the patterns are very similar. The most evident change is over southeast China, followed by the middle east and some locations in Europe and the USA. In 4.11c, the difference between the two scenarios are shown. Here it is seen that one value in the Pacific Ocean overshadows the rest of the change.

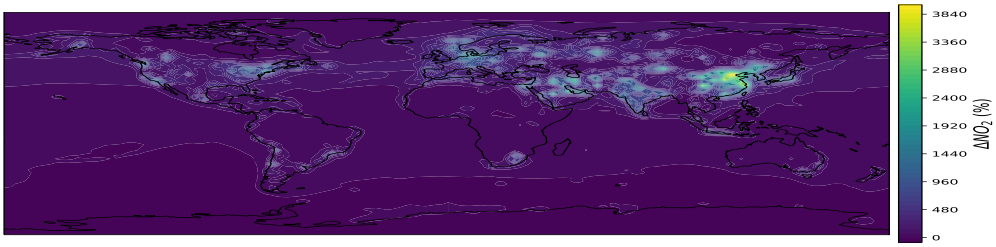

(a) ΔNO_2=2014n-1850n

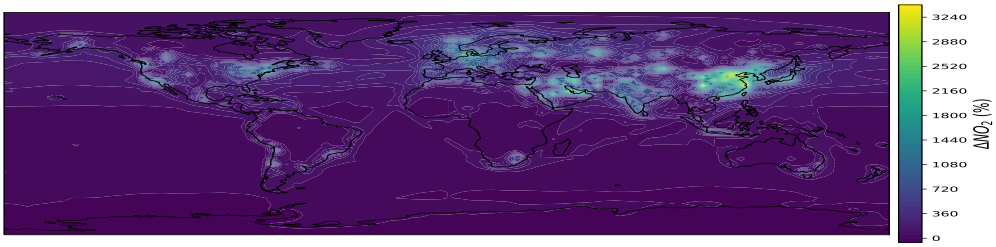

(b) ΔNO_2=2014rN-1850rN

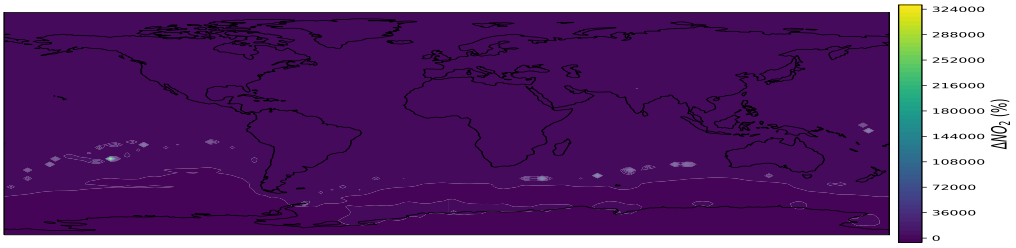

(c) ΔNO_2=|(2014rN-1850rN)|-
|(2014n-1850n)|

Figure 4.11: Total tropospheric column nitrogen dioxide concentration. The figures show the results made by summing over the tropospheric levels and taking the mean over time. The change between 1850 and 2014 for the normal scenario is shown in (a), while (b) show the same change for the rN scenario. The difference in change between the rN scenario and the normal is seen in (c). Note that each part of the figure has its own colour bar, and that these differ.

4.3 Vertical Differences

The third thing interesting to look into is vertical differences. This analysis is interesting because, as described in Figure 2.1, the altitude at which ozone exists determines if it is "good" or "bad" ozone. In this thesis, it is the "good" ozone in the mid-troposphere, which is of concern, because this affects the hydroxyl radical concentration. Additionally, at what altitude nitrogen dioxide exists is important for the ozone concentration, as described in Section 2.1.7. The vertical differences depending on latitude are investigated by comparing the change between 1850 and 2014 for the scenarios. This section presents

the results of this analysis. Results for the hydroxyl radical are not included in this section because the results only showed the same change in some grid boxes, however they are provided Appendix B(Figure B.1). Note also that all values above the defined tropopause(Section 3.4.2) are counted as zero.

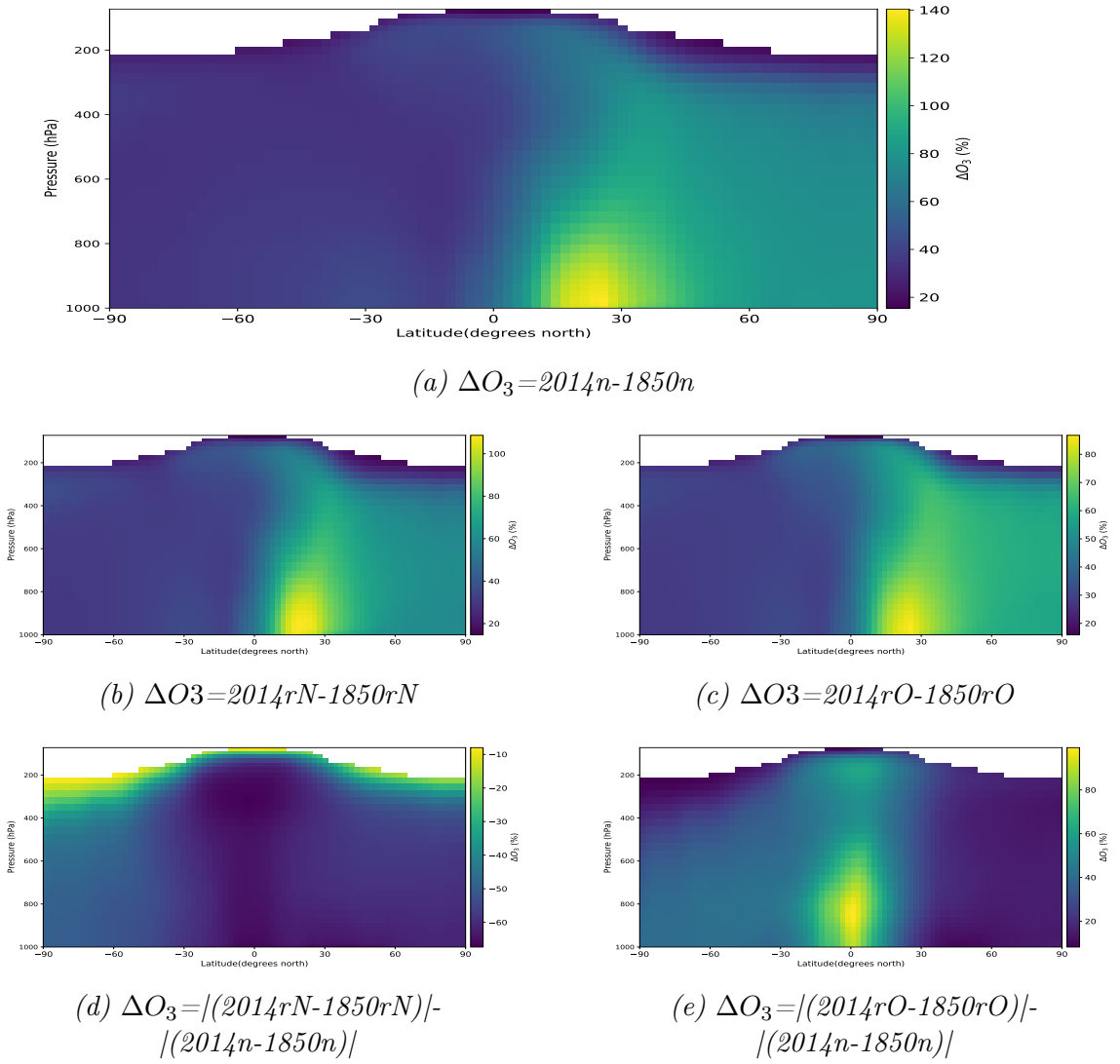

(a) ΔO_3*=2014n-1850n*

(b) $\Delta O3$*=2014rN-1850rN*

(c) $\Delta O3$*=2014rO-1850rO*

(d) ΔO_3*=|(2014rN-1850rN)|-|(2014n-1850n)|*

(e) ΔO_3*=|(2014rO-1850rO)|-|(2014n-1850n)|*

Figure 4.12: Vertical and latitudinal ozone concentration distribution. The change between 1850 and 2014 for the normal scenario is shown in (a), while (b) and (c) show the same change, respectively, for the rN and rO scenarios. The difference in change between the rN and rO scenarios and the normal is seen, respectively, in (d) and (e). Note that each part of the figure has its own colour bar, and that these differ.

Figure 4.12 shows the change in vertical and latitudinal ozone concentration between 1850 to 2014 for the normal and reduced reaction rate scenarios and the difference between them. A similar pattern of change between 1850 and 2014 is seen in all the scenarios, 4.12a-4.12c, with greater change in the northern hemisphere than in the southern. The peak of change is seen just south of 30N from the surface to 800hPa. Close to the top of the tropical tropopause, there are also elevated concentrations. 4.12d shows the difference

between the change in the rN and n scenarios. This difference is more prominent in the northern hemisphere than the southern, with the largest difference found in the tropics. The least difference is found at the top of the troposphere. Considering the difference in change between the rO and n scenarios, seen in 4.12e, the change is greatest in the rO scenario. The difference is most prominent in the southern hemisphere, peaking at the equator from 1000hPa to about 600hPa. Little change is seen close to the tropopause.

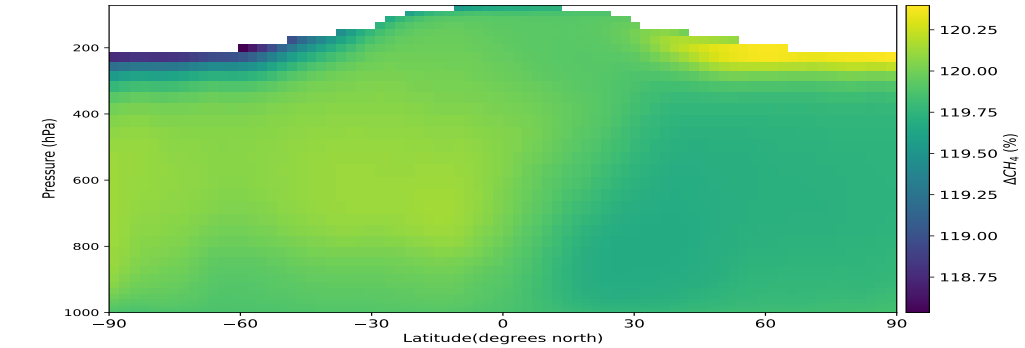

(a) ΔCH_4=2014n-1850n

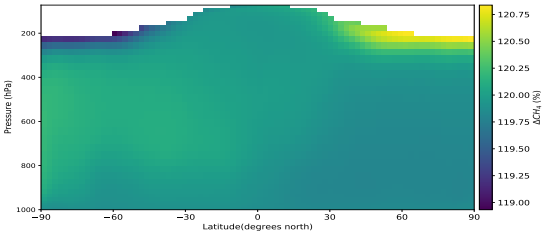

(b) ΔCH_4=2014rN-1850rN

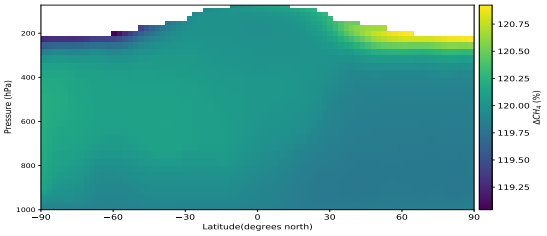

(c) ΔCH_4=2014rO-1850rO

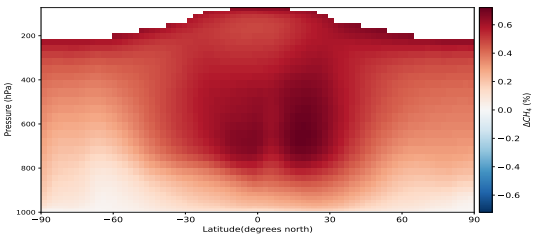

(d) ΔCH_4=|(2014rN-1850rN)|-|(2014n-1850n)|

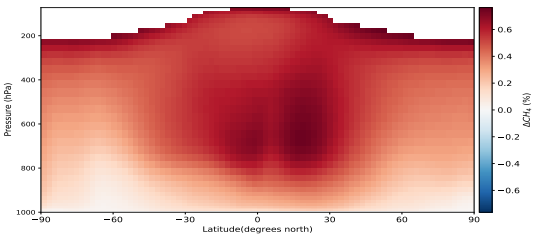

(e) ΔCH_4=|(2014rO-1850rO)|-|(2014n-1850n)|

Figure 4.13: Vertical and latitudinal methane concentration distribution. The change between 1850 and 2014 for the normal scenario is shown in (a), while (b) and (c) show the same change, respectively, for the rN and rO scenarios. The difference in change between the rN and rO scenarios and the normal is seen, respectively, in (d) and (e). Note that each part of the figure has its own colour bar, and that these differ.

Figure 4.13 shows the change in vertical and latitudinal methane concentration between 1850 to 2014 for the reduced reaction rate scenarios, the normal scenario and the difference between them. The change is similar in the three scenarios, with generally higher increase in the southern than in the northern hemisphere, except at the top of the

troposphere where higher values are found in the northern hemisphere and lower values in the southern hemisphere. The differences between the normal and the reduced reaction rate scenarios are seen in 4.13d and 4.13e. Here the most evident difference is seen in the middle to upper troposphere from 30S to 30N, and close to the tropopause through all latitudes. Little difference is seen close to the surface, where the methane field in the model is fixed.

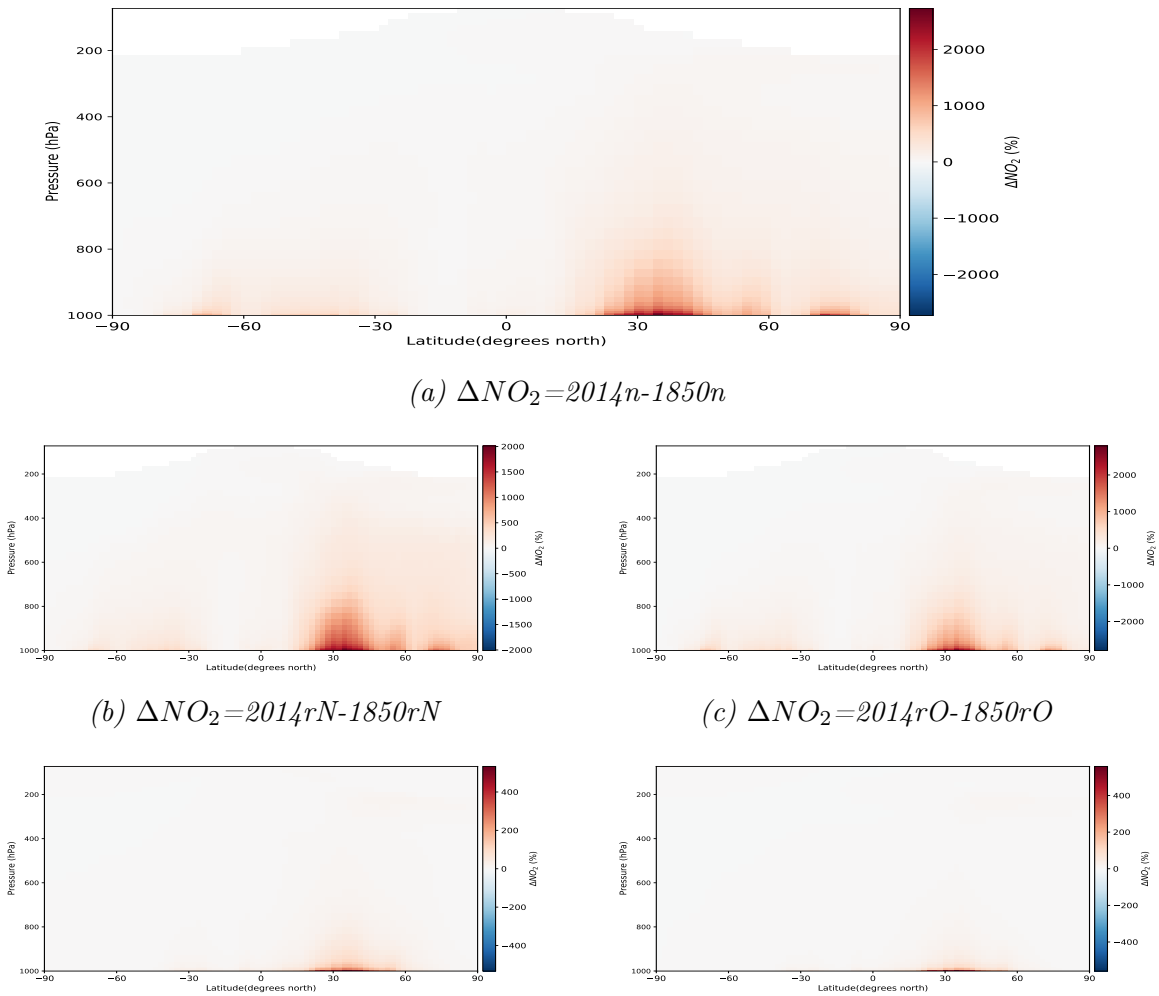

(a) ΔNO_2=2014n-1850n

(b) ΔNO_2=2014rN-1850rN

(c) ΔNO_2=2014rO-1850rO

(d) ΔNO_2=\|(2014rN-1850rN)\|-\|(2014n-1850n)\|

(e) ΔNO_2=\|(2014rO-1850rO)\|-\|(2014n-1850n)\|

Figure 4.14: Vertical and latitudinal nitrogen dioxide concentration distribution. The change between 1850 and 2014 for the normal scenario is shown in (a), while (b) and (c) show the same change, respectively, for the rN and rO scenarios. The difference in change between the rN and rO scenarios and the normal is seen, respectively, in (d) and (e). Note that each part of the figure has its own colour bar, and that these differ.

In Figure 4.14 the change in vertical and latitudinal nitrogen dioxide concentration between 1850 and 2014 for the reduced reaction rate scenarios, the normal scenario and the difference between them are presented. The results in 4.14a-4.14c show very little change between 1850 and 2014, with noticeable change only close to the surface, most

evident around 30N. This change is more prominent in the rN scenario than the two others. In 4.14d-4.14e, it is also seen that the same area is the location of the largest difference between the reduced reaction rate scenarios and the n scenario, with higher concentrations in the former.

4.4 Methane Lifetime

To be able to see the actual change in methane concentration in the reduced reaction rate scenarios, the simulated scenario should have been over a more extended time period, and emissions should have been included. However, looking at the lifetime of methane can give insight into the future development of methane and additionally say something about the concentration of hydroxyl radical. This section presents the methane lifetimes in the three scenarios.

Scenario	1850(s-t)	2014(s-t)	1850(L)	2014(L)
n	7.7	8.1	8.8	8.9
rN	15.5	16.0	18.1	18.4
rO	17.9	18.6	22.3	22.7

Table 4.1: Methane lifetime, given in years, in the different scenarios for 1850 and 2014, rounded to one decimal. The term (s-t) denotes the lifetime calculated for the whole atmosphere, while (L) denotes the Lawrence lifetime, valid below the climatological tropopause.

Table 4.1 shows the lifetime of methane in 1850 and 2014, both for the whole modeled atmosphere(s-t) as well as below the climatological troposphere(L), for the simulated scenarios. It is seen that the methane lifetime, for all the scenarios, is longer when only considering the climatological tropopause. The difference between 1850 and 2014 is larger when accounting for the whole modelled atmosphere than when considering the atmosphere only below the climatological tropopause.

When considering the whole modelled atmosphere, the lifetime of methane is about doubled in the rN scenario for both 1850 and 2014. In the rO scenario, these values are even more elevated. Below the climatological tropopause, in the rN scenario, the lifetime is more than double that in the normal scenario and even higher in the rO scenario. Looking at the difference in lifetime between 1850 and 2014, it is also seen that it increases more in the rN and rO scenarios than in the normal.

4.5 Comparing the Two Experiments

Comparing the results for the two reduced reaction rate scenarios will give some insight into the differences in their effects. The effects on ozone and nitrogen dioxide in the two scenarios are very different; as a result, these species are not considered here. Instead, how the hydroxyl radical and methane are affected is of great interest, especially when

assessing whether or not one of the photochemical reactions is more important than the other concerning hydroxyl radical concentrations and methane lifetime.

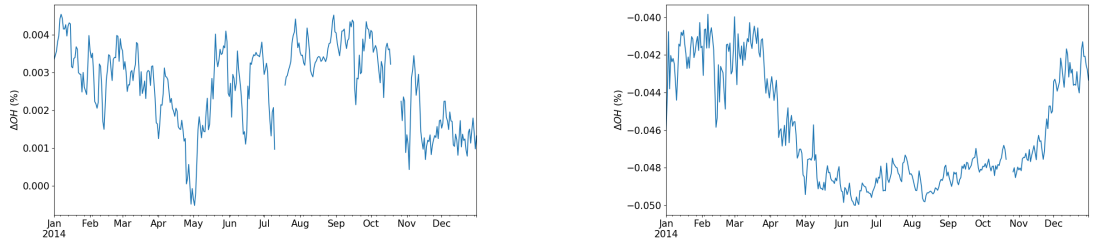

(a) ΔOH=1850rN-1850rO *(b) ΔOH=2014rN-2014rO*

Figure 4.15: Difference in total hydroxyl radical concentration between the rN and rO scenarios. The figures show the results made by summing over latitude, longitude and vertical level and taking the mean over each day.

Figure 4.15 shows the difference in total hydroxyl radical concentration between the *rN* and *rO* scenarios. In 1850, there are higher hydroxyl radical concentrations in the *rN* scenario most of the year, except around May. The lowest difference between the scenarios occurs early winter. In 2014, the situation has changed and there are lower hydroxyl radical concentrations in the *rN* than in the *rO* scenario. The greatest difference is seen during northern hemisphere spring to autumn.

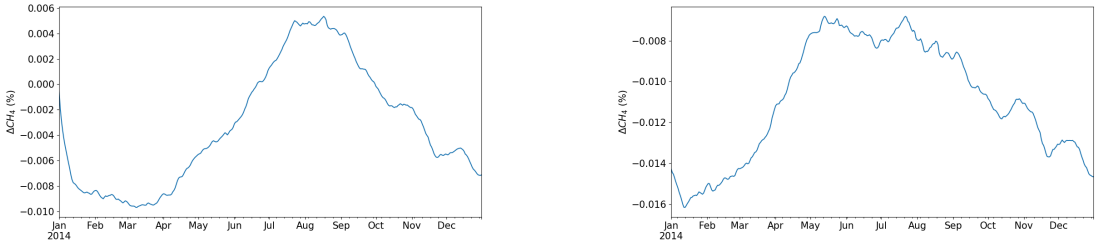

(a) ΔCH_4=1850rN-1850rO *(b) ΔCH_4=2014rN-2014rO*

Figure 4.16: Difference in total methane concentration between the rN and rO scenario. The figures show the results made by summing over latitude, longitude and vertical level and taking the mean over each day.

The difference in total methane concentration between the *rN* and *rO* scenarios is presented in Figure 4.16. In 1850, the methane concentration is lower in the *rN* scenario compared to the *rO* scenario during most of the year, except from June to September. In 2014, the concentration is lower in the *rN* scenario throughout the year, with a peak during January to March.

Chapter 5

Discussion

This chapter discusses the results found in Chapter 4. First, it will look at whether there are differences between the reduced reaction rate scenarios(rN and rO) and the normal scenario. Secondly, it dives into where in the atmosphere these differences occur, to see if it is more prominent at some latitudes or altitudes. Thirdly it considers the results found for the methane lifetime, and consequences of these, before finally discussing the difference between the two reduced reaction rate scenarios.

5.1 Is There a Difference Between the Scenarios?

Whether or not there is a difference between the reduced reaction rate scenarios and the normal scenario is the first thing of interest in this analysis. If there are no differences, the rest of the analysis would be meaningless. This section investigates if these differences exist and discuss the reasons and consequences relevant to this thesis. The analysis is divided into three parts; experiment 1, experiment 2 and differences in 1850 versus 2014. All three parts consider the same question: whether there is a difference in tropospheric concentration of ozone, hydroxyl radical, methane and nitrogen dioxide between the simulations.

5.1.1 Experiment 1

In the rN scenario, the reaction rate of the photochemical reaction

$$\mathrm{NO_2 + hv \xrightarrow{\lambda < 420} NO + O}, \tag{R51}$$

is turned down to 10% of the normal. The results in Section 4.1 shows an increased nitrogen dioxide concentration in the rN scenario(see Figure 4.4 (a) and (c)). This increase is solely an effect of the reduced reaction rate, since the emissions are the same as in the normal scenario. As explained in Section 2.1.7, the Reaction (R51) is not a NO_x sink, only a transfer between nitrogen dioxide and nitrogen monoxide. The resulting assumption being that the difference in NO_x is mainly the ratio between its components, higher fraction of nitrogen dioxide to nitrogen monoxide, not necessarily in its total concentration. However, as seen in Section 2.1.7.2, the loss of NO_x starts with nitrogen dioxide reacting, which could mean that the loss could increase with the changed ratio between

nitrogen dioxide and nitrogen monoxide. The question of interest here is how this change affects the ozone concentration.

Reaction (R51) is the primary source of tropospheric ozone(Jacob, 1999), and the reduced reaction rate would immediately be associated with a reduction in the ozone concentration. However, if this means that the nitrogen dioxide concentration increases and the NO_x sink does not change, the abundance of nitrogen dioxide might become large enough to compensate for some of the reduction in the reaction rate. In addition, when considering the ozone sinks, an increase in NO_x could mean a decrease in these, because ozone loss is larger in low NO_x environments(Jacob, 1999). On the other hand, if it means that the NO_x sinks increases, the reduction reaches its full potential of affecting the ozone concentration, not only due to the reduced reaction rate but loss of nitrogen dioxide during night also consumes ozone(Jacob, 1999). The change in ozone concentration resulting from the reduction in the reaction rate of (R51) is presented in Figure 4.1a (a) and (c). It is evident that the ozone concentration is lower in the *rN* scenario, meaning that the increase in nitrogen dioxide is not enough to compensate, at least fully, for the reduced reaction rate. This reduction in ozone concentration could result in a reduction in the NO_x sinks during night, where it participates in the conversion from nitrogen dioxide to nitric acid. In addition it could influence the cycling between nitrogen monoxide and nitrogen dioxide because it participates in the conversion from nitrogen monoxide to nitrogen dioxide.

Another consequence of a reduction in ozone concentration is that the production of tropospheric hydroxyl radical is affected. The hydroxyl radical is the most important tropospheric oxidant, and how it is affected by the reduction in the reaction rate of Reaction (R51) is one of the main interests in this thesis. Tropospheric production of the hydroxyl radical takes place mainly by photodissociation of ozone(Jacob, 1999). As aforementioned, the ozone concentration is lower in the *rN* scenario than in the normal, resulting in a reduction in hydroxyl radical formation. In addition the hydroxyl radical recycling mechanisms(Lelieveld et al., 2016), explained in Section 2.1.5.1, are affected both by the reduction in ozone concentration and the possible change in ration between nitrogen dioxide and nitrogen monoxide. The O_x- and NO_x recycling mechanisms depend on the abundance, respectively, of ozone and nitrogen monoxide(Lelieveld et al., 2016), and a reduction in these would decrease the recycling efficiency. The hydroxyl radical sinks are also affected by a change in the ratio between nitrogen monoxide and nitrogen dioxide. In very high NO_x environments nitrogen dioxide is a sink for the hydroxyl radical(Jacob, 1999), so an increase in nitrogen dioxide could increase the effect of this sink. How many hydroxyl radicals are lost by oxidation of trace gases, largely depends on the amount of nitrogen monoxide present(see Section 2.1.5.2), and a reduction in nitrogen monoxide would make these oxidation processes a larger hydroxyl radical sink. Figure 4.2a shows that there is indeed lower hydroxyl radical concentration in the *rN* scenario than in the normal.

This reduction in hydroxyl radical concentration can again impact the NO_x ratio and the ozone concentration. The production of ozone is initiated by a hydrocarbon reacting with a hydroxyl radical, which later on produces nitrogen dioxide, which goes into Reaction (R51) to produce ozone(Jacob, 1999). In addition, the loss of NO_x during daytime is through hydroxyl radicals reacting with nitrogen dioxide, and a reduction in hydroxyl radical concentration would make this sink smaller.

Oxidation by the hydroxyl radical is the main sink for methane(Saunois et al., 2016).

Hence, a reduction in hydroxyl radical concentration will also lead to a reduction in the methane sink, increasing its atmospheric concentration. Figure 4.3 (a) and (c) shows that the methane concentration indeed is higher in the *rN* scenario than in the normal.

5.1.2 Experiment 2

In Experiment 2, the *rO* experiment, the reaction rate of the photochemical reaction

$$O_3 + hv \xrightarrow{300nm < \lambda < 320nm} O_2 + O(^1D), \tag{R52}$$

is reduced to 10% of its normal value. In this scenario, the only change is the reaction rate of reaction (R52), which is an important sink for ozone(Jacob, 1999), so it is expected that the ozone concentration in this scenario is higher than in the normal one. However, another possibility is that other ozone sinks could compensate for the decrease in the photodissociation loss. The results in Section 4.1 shows that the ozone concentration is in fact elevated in the *rO* scenario, compared to the *n* scenario(see Figure 4.1 (b) and (d)). This finding means that the other ozone sinks are not able to compensate for the reduced reaction rate of R52. An increase in the ozone concentration will impact the NO_x ratio as well(Jacob, 1999), as more ozone is available to react with nitrogen monoxide to produce nitrogen dioxide. In addition, the NO_x concentration could be impacted by this change as well, due to more ozone available to NO_x loss during the night.

The nitrogen dioxide concentration in the *rO* scenario is found to be lower during some periods and higher during other. In 2014 the period of elevated values is from May to October, while in 1850 from July to September. The increase in nitrogen dioxide concentration during northern hemisphere spring to autumn could be a result of a shift in the ratio between nitrogen dioxide and nitrogen monoxide, due to more ozone available for reaction with nitrogen monoxide to produce nitrogen dioxide. The lower values during northern hemisphere late autumn to early spring, on the other hand, could implicate that the increased ozone concentration positively affects the nightly NO_x loss. To be able to say anything certain about the effect on NO_x concentration, an analysis of nitrogen monoxide would also be needed. However, it is a fair assumption that the concentration decreases and the ratio between nitrogen dioxide and nitrogen monoxide shifts towards nitrogen dioxide, as a result of the increased ozone concentration.

A decrease in the reaction rate of reaction (R52) could also heavily affect the hydroxyl radical concentration, as it is the primary production of hydroxyl radical. However, because the ozone concentration increase, this could compensate for the reduced reaction rate. The concentration of nitrogen dioxide has also been found to be lower in the *rO* scenario during late autumn to early spring in 2014 and most of the year except mid-summer to early spring in 1850. Assuming the total NO_x concentrations are lower in the *rO* scenario, with a shift in the ratio between nitrogen monoxide and nitrogen monoxide in favour of nitrogen dioxide, the NO_x recycling mechanism(Lelieveld et al., 2016) would decrease as well. As a result of this decreased NO_x recycling mechanism, more hydroxyl radical could be lost during oxidation of carbon monoxide. On the other hand, the increased ozone concentration could make the O_x recycling mechanism(Lelieveld et al., 2016) more efficient. Hydroxyl radical loss during daytime, where hydroxyl reacts with nitrogen dioxide to form nitric acid(Jacob, 1999), could also be altered by the change in nitrogen dioxide concentration. Figure 4.2b and 4.2d shows that the hydroxyl radical

concentration is generally lower in the rO scenario than in the normal. This finding means that the mechanisms leading to a decreased hydroxyl radical production or recycling surpasses the ones which could lead to an increase in hydroxyl radical concentration. The only exception is some periods during June to October in 2014, which could mean that the increase in ozone concentration during northern hemisphere summer and autumn can compensate for the reduction of the reaction rate of reaction (R52).

Reduction in the hydroxyl radical concentration have many consequences; loss of ozone in very low NO_x environments reduces, less nitrogen monoxide will react to produce nitrogen dioxide and the NO_x loss during daytime reduces(Jacob, 1999). In addition, the loss of methane will decrease, this is seen by the higher methane concentrations found in 4.3b-4.3d. Increasing methane concentrations will lead to additional decrease in the hydroxyl radical concentration, and thereby increase its own lifetime.

5.1.3 Comparing Differences in 1850 to 2014

Hypothesis one in section 3.3.3 was that the difference between the scenarios would be more prominent in 2014 than in 1850. The reason for this hypothesis is that the emissions of methane and nitrogen dioxide have increased from 1850 to 2014(Nicely et al., 2018; Young et al., 2013). These gases have opposite effects when considering the hydroxyl radical, where methane acts as the second most important sink, and nitrogen dioxide is important for ozone production, which is the primary source of hydroxyl radical(Jacob, 1999).

Both in the rN and rO scenarios the difference to the n scenario is greater in 2014 compared to 1850 for all considered species.

5.2 Global Distribution

Having found a difference between the scenarios, the analysis can continue. This section considers the global distribution of the differences. The difference in the global distribution of ozone, hydroxyl radical, methane and nitrogen dioxide between the scenarios are assumed more prominent in lower latitudes and regions with high NO_x emissions, since the controlling effects are the abundance of NO_x and solar insolation(Jacob, 1999). Emissions of NO_x ha shifted from North America and Europe to Asia since the 1990s(Gaudel et al., 2018), so the differences in 2014 are expected to be most prominent in Asian low latitudes.

5.2.1 Experiment 1

The time-mean total latitudinal difference in nitrogen dioxide concentration between scenario rN and n(Figure 4.8d) is found to be most prominent in the northern hemisphere with a peak around 30N. On the southern hemisphere, little difference is seen. The total tropospheric column difference(Figure 4.11c) does not show much.

Because ozone production is dependent on nitrogen dioxide concentration(Jacob, 1999) it is expected that the largest difference in ozone concentration between the rN and n scenario is occurring at the same latitudes and locations as nitrogen dioxide. Figure 4.5d shows that also the difference in ozone concentration is largest around northern

hemisphere mid latitudes. This finding is confirmed by Figure 4.9d, which also shows larger differences in the northern hemisphere. In the latter it is also seen that the peak of the change is in southern Asia, where the highest NO_x emissions are found(Gaudel et al., 2018).

Considering the hydroxyl radical concentration, which is dependent on the ozone concentration, the largest change should be found where the largest change is seen in the ozone concentration. This is not what is seen in the results in Figure 4.6d; rather, the largest difference is seen close to the poles. Taking a closer look at the difference in total column concentration for ozone(Figure 4.9d) and methane(Figure 4.10d) it is seen that the ozone concentration is slightly lower and the methane concentration slightly higher close to the poles in the rN than in the n scenario. One resulting possible explanation is that these small changes in ozone concentrations at latitudes with little solar insolation has a much higher impact on the hydroxyl radical concentration than larger changes at latitudes with higher solar insolation. Another explanation is that these results do not capture the actual situation in the scenario.

Figure 4.7d shows that the difference in methane concentration is largest in low latitudes. However, as methane is a well-mixed greenhouse gas(Myhre et al., 2013), the concentration is quite similar all over the world, and the largest difference is expected to be found where the tropospheric column is the highest. As the defined tropopause(see Section 3.4.2) is highest in low latitudes(Graversen et al., 2014), this result is not particularly surprising. The total tropospheric column difference, seen in Figure 4.10d reveals some additional information. This result shows that the difference in methane concentration is larger at about the same place as for ozone, over southern Asia, however, with a larger spatial spread.

5.2.2 Experiment 2

The difference in mean latitudinal change in ozone concentration from 1850 to 2014 between the rO and n scenario, seen in Figure 4.5e, shows that the largest difference is found at low northern latitudes. This finding is supported by the results in the total column result(Figure 4.9e) where it is also seen that the difference is most prominent over the pacific ocean. Compared to the results in Experiment 1, this difference is closer to the equator, and could be due to the difference in wavelength needed in the two photochemical reactions (R51)-(R52), where the upper limit for ozone to photodissociate is lower than for nitrogen dioxide(Jacob, 1999). In the tropics, the ozone layer is relatively thin, allowing more UV radiation to penetrate to the troposphere, resulting in high insolation and water vapour concentration(Lelieveld et al., 2016).

An increase in the ozone concentration would also affect the nitrogen dioxide concentration. In the rO scenario, the difference in the latitudinal nitrogen dioxide concentration, seen in Figure 4.8e, is small, especially in the southern hemisphere. In the northern hemisphere there is found a peak with higher concentrations in the rO scenario around 30N, and lower values in the rO scenario than the normal from about 40N-90N. A probable reason for the 30N peak is that there are more ozone available to react with nitrogen monoxide to produce nitrogen dioxide, while between 40-90N there is more ozone available to react with nitrogen dioxide during night to form nitric acid.

The difference in mean latitudinal change in hydroxyl radical concentration from 1850

to 2014 between the rO and the n scenario shows the same pattern as in Experiment 1. However, the same(possible) explanation cannot be used, since the change in ozone concentration is higher in the rO scenario than in the n over the whole globe. What the explanation can be is that the increase in ozone near the poles are not very high, so that there is less to compensate for the reduced reaction rate. However, also here, the explanation could be that these results do not capture the actual situation in the scenario.

Considering the difference in the latitudinal change in methane concentration, this is similar to the one for the rN scenario, only slightly higher, and the same arguments as for Experiment 1 are valid.

5.3 Vertical Differences

Vertical change in concentration of the considered species is of great interest. At which tropospheric altitude ozone exist determines whether it is "good" or "bad" ozone(Jacob, 1999), and at which altitude nitrogen dioxide exists affects where ozone is produced. These factors again determine at which degree the production of hydroxyl radicals is affected. This section contains the discussion of the results found for vertical differences.

5.3.1 Experiment 1

It is seen from Figure 4.14d that the only noticeable difference in nitrogen dioxide concentration is found close to the surface around 30N, with a more significant change in the rN scenario than in the normal. This area is also found to be the place where the change between 1850-2014 is most prominent in both the normal and rN scenario.

As aforementioned, where in the troposphere the ozone change happens is of great importance for how the hydroxyl radical is affected. If the largest change is close to the surface, it would mean less of the "bad" ozone, which is toxic to biological tissue, in the middle troposphere, it would mean less hydroxyl radical production, while in the upper troposphere, it would mean less effect on global warming(Jacob, 1999). It is expected that the difference somewhat follows that seen for nitrogen dioxide. Figure 4.12d shows the difference in ozone concentration over pressure level and latitudes. Least difference is seen close to the tropopause, which either means that there is less ozone contributing to global warming, or that the defined tropopause is slightly too high so that this is in fact changes in the stratosphere. The largest difference is found around equator from the surface almost to the tropopause, and it is generally more prominent in the northern than in the southern hemisphere. This means that there is less ozone contributing to hydroxyl radical production and surface pollution. The production of the hydroxyl radical is not only dependent on the ozone concentration, but also the amount of solar insolation and water vapour. The mid tropical troposphere has the best conditions for hydroxyl radical production due to a thin ozone layer allowing for more insolation in the right wavelengths and high water vapour concentrations. So, the difference in ozone concentration in this area is of great importance. It is seen that there are notably less ozone in this region, which would affect the hydroxyl radical concentration negatively.

Methane is a well-mixed greenhouse gas, so it is expected that its concentration is quite similar throughout the troposphere. However, if the effect of reduced ozone on the hydroxyl radical concentration is spatially very variable, the difference could be noticeable.

Figure 4.13d shows that a difference indeed can be seen. It is not a very big difference, but it is most prominent in the mid and upper tropical troposphere. The difference is also larger in the northern than the southern hemisphere, where it also stretches to the subtropics. No difference between the *rN* and *n* scenario is seen at the surface, where the methane field in the Oslo CTM3 is kept constant.

5.3.2 Experiment 2

The vertical difference in ozone concentration between the *rO* and *n* scenarios is more prominent in the southern than in the northern hemisphere. A peak in the difference is found at the equator, from 1000hPa to about 600hPa. Also, elevated values are found nearly up to the troposphere. This area where the difference in ozone concentration is most prominent is an area where solar insolation with the right wavelengths for ozone photodissociation is substantial(Lelieveld et al., 2016). The peak of change here can be explained as a result of the reduction in the reaction rate is most affected in the area where it happens the most. Considering whether it is *good* or *bad* ozone that increases in magnitude, it is seen that the elevation in the lower mid-troposphere increases, which leads to additional hydroxyl radical production. In contrast, the elevation close to the tropopause leads to an intensified greenhouse effect.

Changes in the ozone concentration affects the nitrogen dioxide concentration. From Figure 4.14e, it is seen that the difference in change between 1850 to 2014 between the *rO* and n scenarios is only noticeable close to the surface around 30N. This result is not as expected, considering the change in ozone concentration, the problem might be that the high values near the surface at 30N so high that they overshadow other changes.

The results for methane are similar as for Experiment 1, and the same arguments are valid.

5.4 Methane Lifetime

Determining the difference in methane lifetime between the scenarios is important to be able to say something about how the evolution beyond the one-year simulations would be. Methane concentrations have been found to be elevated in the reduced reaction rate scenarios compared to the normal. As methane affects its own lifetime by the fact that it alters the lifetime of its own largest sink, the hydroxyl radical(Myhre et al., 2013), its lifetime is expected to be longer in the reduced reaction rate scenario than in the normal scenario.

Table 4.1 presented the methane lifetime results for the three scenarios. The first thing to note is how the 2014 lifetimes in the normal scenario of methane compare to results found by others. Voulgarak et al. (2013) found the methane lifetime to oxidation by the hydroxyl radical to be 9.8±1.6 from a ACCMIP multi-model mean. For the whole modelled atmosphere in the Oslo CTM3, the methane lifetime is slightly below the ACCMIP multi-model mean, while when only considering the climatological troposphere the lifetime is just within.

The difference between the scenarios is similar for the whole modelled atmosphere and the climatological troposphere. In the *rN* scenario, the lifetime of methane is about twice that of the normal, both in 1850 and 2014. While in the *rO* scenario, the results

show an even more evident elevation. These results confirm that the hydroxyl radical concentration has decreased in the reduced reaction rate scenarios, because the methane field has not been altered, nor has the other methane sinks. The changes in reaction rates affect the hydroxyl radical concentration and hence the methane lifetime. If simulated further in time, it would be expected that this increased methane lifetime would lead to higher concentrations, reduced hydroxyl radical concentrations and further increased methane lifetime.

The methane lifetime increases more in the reduced reaction rate scenarios than in the normal. This result indicates that the change in the hydroxyl radical concentration between 1850 and 2014 has increased less in the reduced reaction rate scenarios compared to the normal. There are also differences in the increase between 1850 to 2014 between the whole modelled atmosphere and the climatological troposphere. For all scenarios, this change is more significant when considering the whole modelled atmosphere.

Comparing the methane lifetimes in the whole modeled atmosphere to the climatological troposphere shows that they are higher in the climatological troposphere, and that the difference between the scenarios also are higher here. The scenarios in this thesis only contain changes the tropospheric chemistry, in addition 85% of the atmospheric mass is within the troposphere(Jacob, 1999). For these reasons it is not surprising that the differences are more evident in the climatological troposphere.

5.5 Comparing the Two Experiments

In 1850 there are higher hydroxyl radical concentrations in the *rN* scenario compared to the *rO* scenario most of the year, except during May, while in 2014 there are lower values throughout the year, most prominent during May to November. The methane concentration in 1850 is higher in the *rN* scenario than the *rO* scenario, except during northern hemisphere summer to early autumn. In 2014 there are higher methane concentration throughout the year in the *rO* scenario than in the *rN* scenario. These results seem counter-intuitive because a higher hydroxyl radical concentration would mean a higher methane sink. The reason behind these results are not apparent, it could be due to an error in the simulation or the analysis, or some other mechanism not considered here.

Table 5.1 shows the percent difference in methane lifetime comparing the reduced reaction rate scenarios to the normal scenario. For both scenarios the difference is largest in 1850, and within the climatological troposphere. The difference is most prominent in the *rO* scenario, both in the year 1850 and 2014 for the whole modelled atmosphere and only considering the climatological tropopause. This difference implicates that the hydroxyl radical concentration is, in fact, most affected in the *rO* scenario.

5.6 Limitations

There are some limitations in this thesis concerning the accuracy in the analysis. This section will discuss and propose ways to solve some of these.

In the simulations, the meteorological year 2014 has been used as input both for 1850 and 2014. This choice was made to better single out the differences occurring due to the changed reaction rates. However, the results for the analysis does not represent the

Scenario	1850(s-t)	2014(s-t)	1850(L)	2014(L)
rN	+ 101%	+ 97%	+ 106%	+ 107%
rO	+ 133%	+ 130%	+ 153%	+ 155%

Table 5.1: Increase in methane lifetime, given in percentage, in the reduced reaction rate scenarios compared to the normal scenario. (s-t) denotes the lifetime calculated for the whole atmosphere, while (L) denotes the Lawrence lifetime, valid below the climatological tropopause. These values are calculated from the results in Table 4.1.

actual conditions for the year 1850. Additionally, the Oslo CTM3 was run with a fixed methane field, not emissions, also to single out the effect of the changed reaction rates. This choice results in no, or little, the difference in the methane concentration near the surface between the scenarios.

During the preprocessing of the data from the Oslo CTM3 simulations, the climatological tropopause was defined, inspired by results from Graversen et al. (2014). This definition might not be accurate for the simulations conducted in this thesis, as the height of the troposphere depends on multiple factors. The result of this simplification is that somewhere or sometimes values counted as tropospheric might include some values which are, in fact, stratospheric, or some actual tropospheric values are lost to the stratosphere. A better way to define the tropopause is to calculate it from the meteorological data, this would ensure that all tropospheric values are included while no stratospheric.

In the analysis, some problems were encountered considering the hydroxyl radical and nitrogen dioxide in the *rO* scenario. When calculating the mean over any dimension in the data set, some of the values became infinite. This problem was solved by replacing these values with *Not a Number*(NaN), which were then ignored when calculating the mean values. However, this leads to missing results for total concentration for the affected species and might have resulted in errors in the results for latitudinal and vertical changes and differences. Why this problem occurred is uncertain; nevertheless, it is certain that the values are not infinite as low values were expected.

Chapter 6

Conclusions and Future Work

This thesis was triggered by curiosity as to the recent methane evolution, which after a ten-year period of stabilization resumed its growth for reasons not well understood(e.g., Turner et al., 2017; McNorton et al., 2016 and Nisbet et al., 2019). The reason for this evolution could be due to changes in methane sources, sinks or both. If the explanation for the resumed methane growth is a reduction in its sinks, the consequences would be serious indeed(Nisbet et al., 2016), a possibility which motivated this investigation.

The hydroxyl radical is the most important tropospheric oxidant and the main sink for methane. For the concentration of the hydroxyl radical, photochemical reactions are essential, and the aim of this thesis was to investigate the importance of the following photochemical reactions on the tropospheric concentration of ozone, the hydroxyl radical and methane:

$$NO_2 + hv \xrightarrow{\lambda 430nm} NO + O, \tag{R53}$$

$$O_3 + hv \xrightarrow{300nm < \lambda < 320nm} O_2 + O(^1D). \tag{R54}$$

Two research questions were constructed in conjunction with the investigation:

1. What would the evolution, from pre-industrial to present day, of ozone, hydroxyl radical and methane concentrations and the lifetime of methane have looked if one of the reactions (R1)-(R2) had a lower reaction rate in contrast to how that evolution has actually played out?

2. Is it possible that one of the two reactions, (R1)-(R2), is more important than the other with respect to the hydroxyl radical concentration and methane lifetime?

To answer these questions a counterfactual investigation was performed. Two experiments were conducted by simulations with the Oslo CTM3: Experiment 1 where the reaction rate of (R53) was slowed by 90% and Experiment 2 where the reaction rate of (R54) was slowed by 90%. A reference scenario with normal chemistry was also simulated. All three scenarios were simulated for the years 1850 and 2014, to illustrate pre-industrial and present day conditions. A schematic illustration of the experiments is shown in Table 6.1. Along the way, it became evident that it would be wise to include nitrogen dioxide in the analysis along with ozone, hydroxyl radical and methane, because it affects many of the relevant processes.

Scenario	1850	2014
Normal reaction rate	$O_3 + hv \xrightarrow{300 < \lambda < 320nm} O_2 + O(^1D)$	$O_3 + hv \xrightarrow{300 < \lambda < 320nm} O_2 + O(^1D)$
rN	$(NO_2 + hv \xrightarrow{\lambda 430nm} NO + O) \times 0.1$	$(NO_2 + hv \xrightarrow{\lambda 430nm} NO + O) \times 0.1$
rO	$(O_3 + hv \xrightarrow{300 < \lambda < 320nm} O_2 + O(^1D)) \times 0.1$	$(O_3 + hv \xrightarrow{300 < \lambda < 320nm} O_2 + O(^1D)) \times 0.1$

Table 6.1: Schematic illustration of the simulated experiments. Experiment 1 is denoted rN and Experiment 2 as rO.

This chapter will reveal whether the research questions have been answered, and if so, what those answers are. In addition, a review of the hypotheses is provided. Finally there are suggestions for future work.

6.1 Conclusions

A counterfactual investigation of the importance of photochemical reactions for the hydroxyl radical concentration and methane lifetime has been conducted. The results from this analysis showed that the hydroxyl radical concentration decreases, and the methane lifetime increases if photodissociation of either ozone *or* nitrogen dioxide slows. Following are the answers to the research questions constructed in this thesis.

- What would the evolution, from pre-industrial to present day, of ozone, hydroxyl radical and methane concentrations and the lifetime of methane have looked if one of the reactions (R1)-(R2) had a lower reaction rate in contrast to how that evolution has actually played out?
  - The change in ozone concentration is reduced if the reaction rate of reaction (R53) is reduced, most noticeable around 30N and evenly distributed at all pressure levels. If the reaction rate of reaction (R54) is reduced, on the other hand, the ozone concentration change increases, most prominently at 30N, evenly distributed at all pressure levels except for a peak from the surface at the equator to about 600hPa.
  - Hydroxyl radical concentration change decreases if either of the reaction rates is reduced. This change is found to be most prominent close to the poles.
  - Methane concentration change increases if either of the reaction rates is reduced. The change is most prominent at low latitudes and in the middle to upper troposphere.
  - The change in methane lifetime from 1850 to 2014 increases if either of the reaction rates is reduced.
- Is it possible that one of the two reactions, (R1)-(R2), is more important than the other with respect to the hydroxyl radical concentration and methane lifetime?

- The hydroxyl radical concentration is higher in 1850 when the reaction rate of reaction (R53) is reduced compared to reaction (R54), while in 2014 it is the opposite.
- Methane concentrations are higher in 1850 when reducing the reaction rate of reaction (R53) compared to reaction(R54), while the opposite is true for 2014.
- The lifetime of methane increases more when the reaction rate of reaction(R54) is reduced, compared to reaction(R53). Additionally, the difference in lifetime between 1850 and 2014 is most prominent when reducing the reaction rate of reaction(R54).

During the analysis, it became evident that consideration of the nitrogen dioxide concentration was essential, as it is important not only for the production of ozone, but also for the concentrations of both ozone and the hydroxyl radical. In both reduced reaction rate scenarios, the differences with respect to the normal scenario were most prominent in the northern hemisphere with a peak of positive difference around 30N and close to the surface. The nitrogen dioxide concentration was higher in the rN scenario at all latitudes compared to the normal scenario, while in the rO scenario, it was lower from about 40-90N.

The differences between the reduced reaction rate scenarios and the normal scenario were found to be more prominent in 2014 compared to 1850. This finding supports the hypothesis of a more evident change when the concentrations and emissions of methane and nitrogen dioxide are more significant.

6.2 Future Work

The process of posing and answering research questions typically generates additional questions and ideas that need to be explored through further research. This thesis explored the importance of photochemical reactions to the hydroxyl radical concentration and methane lifetime through a counterfactual investigation.

Photochemical reactions are dependent on solar insolation, so it would be intriguing to analyse the seasonal differences between the scenarios.

In this thesis, there have been speculations on the ratio of nitrogen dioxide to nitrogen monoxide, and how it changes in the experiments. However, due to time limitations, only nitrogen dioxide has been considered. It would be interesting to look further into what happens to NO_x in the experiments. To do this, nitrogen dioxide, nitrogen monoxide and nitric acid should be investigated to determine what happens to the ratio of the NO_x family members, and if the NO_x sink, to nitric acid, is affected.

As described in Section 2.1.5.2, carbon monoxide is the largest hydroxyl radical sink in the troposphere, so reduced hydroxyl radical concentrations would affect carbon monoxide concentrations as well. When carbon monoxide is oxidized, the result is carbon dioxide, so analyzing carbon monoxide and carbon dioxide in both experiments would also be of interest.

Ideas for other simulations and scenarios in relation to the conducted scenarios have arisen during this work:

- A large increase in methane lifetime was found in this work, which has consequences for methane and hydroxyl radical concentrations. It would be fascinating to look at how this would evolve, keeping the changes in one of the reaction rates for Reaction (R53)/(R54). This can be done either by simulating for multiple years or by increasing the methane concentration in the model. One possible consequence could be depletion of the hydroxyl radical.

- Another possibility would be simulating the scenarios with methane emissions instead of fixed surface methane fields.

- Because both scenarios considered in this thesis showed a large increase in methane lifetime, simulating an additional experiment where both the reaction rates are slowed would be interesting. The consequences of this scenario would probably be serious.

- Simulating a scenario with reduced NO_x emissions to compare the effects on ozone, the hydroxyl radical and methane, to the *rN* scenario simulated in this thesis could be intriguing.

Bibliography

Brasseur, G. P. and Jacob D. J. (2017). *Modeling of Atmospheric Chemistry*. Cambridge University Press. DOI: 10.1017/9781316544754.

Ciais, P. et al. (2013). In: *Climate Change 2013: The Physical Science Basis. Contribution of Working Group I to the Fifth Assessment Report of the Intergovernmental Panel on Climate Change*. Cambridge University Press. Chap. 6, pp. 465–570.

Dalsøren, S. et al. (2016). "Atmospheric methane evolution the last 40 years". In: *Atmospheric Chemistry and Physics* 16, pp. 3099–3126. DOI: 10.5194/acp-16-3099-2016.

Delmas, R., Serça D., and Jambert C. (1997). "Global inventory of NO x sources". In: *Nutrient cycling in agroecosystems* 48(1-2), pp. 51–60. DOI: 10.1023/A:1009793806086.

Falk, S. (2020a). Personal communication. Postdoctoral Fellow, Section for Meteorology and Oceanography, University of Oslo.

— (2020b). *How to do pre industrial runs with CTM3*. URL: https://github.com/NordicESMhub/OsloCTM3/wiki/How-to-do-pre-industrial-runs-with-CTM3. (accessed: 21.07.2020).

Gaudel, A. et al. (2018). "Tropospheric Ozone Assessment Report: Present-day distribution and trends of tropospheric ozone relevant to climate and global atmospheric chemistry model evaluation". In: *Elementa: Science of the Anthropocene* 6(1). DOI: 10.1525/elementa.291.

Goll, D. S. et al. (2014). "Climate-driven changes in chemical weathering and associated phosphorus release since 1850: Implications for the land carbon balance". In: *Geophysical Research Letters* 41(10), pp. 3553–3558. DOI: 10.1002/2014GL059471.

Graversen, R. G., Langen P. L., and Mauritsen T. (2014). "Polar amplification in CCSM4: Contributions from the lapse rate and surface albedo feedbacks". In: *Journal of Climate* 27(12), pp. 4433–4450. DOI: 10.1175/JCLI-D-13-00551.1.

Hartmann, D.L. et al. (2013). "Observations: Atmosphere and Surface". In: *Climate Change 2013: The Physical Science Basis. Contribution of Working Group I to the Fifth Assessment Report of the Intergovernmental Panel on Climate Change*. Cambridge University Press. Chap. 2, pp. 159–254.

Haslerud, A. S. (2018). *Oslo CTM3 User Manual*. v1.0. CICERO Center for International Climate Research. URL: https://osloctm3-docs.readthedocs.io/en/latest/manual_osloctm3.html.

Hesstvedt, E., Hov Ø., and Isaksen I. S. A. (1978). "Quasi-steady-state approximations in air pollution modeling: Comparison of two numerical schemes for oxidant prediction". In: *International Journal of Chemical Kinetics* 10(9), pp. 971–994. DOI: 10.1002/kin.550100907.

Hoesly, R. M. et al. (2018). "Historical (1750-2014) anthropogenic emissions of reactive gases and aerosols from the Community Emission Data System (CEDS)". In: *Geoscientific Model Development* 11, pp. 369–408. DOI: 10.5194/gmd-11-369-2018.

Holtslag, A. A. M., De Bruijn E. I. F., and Pan H. L. (1990). "A high resolution air mass transformation model for short-range weather forecasting". In: *Monthly Weather Review* 118(8), pp. 1561–1575. DOI: 10.1175/1520-0493(1990)118<1561:AHRAMT>2.0.CO;2.

Jacob, D. J. (1999). *Introduction to atmospheric chemistry*. New Jersey: Princeton University Press.

Kennedy, C. (2015). *2014 State of the Climate: Carbon Dioxide*. URL: https://www.climate.gov/news-features/understanding-climate/2014-state-climate-carbon-dioxide. (accessed: 10.08.2020).

Krause, A. et al. (2014). "The sensitivity of global wildfires to simulated past, present, and future lightning frequency". In: *Journal of Geophysical Research: Biogeosciences* 119(3), pp. 312–322. DOI: 10.1002/2013JG002502.

Krol, M. C. et al. (2003). "Continuing emissions of methyl chloroform from Europe". In: *Nature* 421(6919), pp. 131–135. DOI: 10.1038/nature01311.

Lamarque, J. F. et al. (2012). "The Atmospheric Chemistry and Climate Model Intercomparison Project (ACCMIP): overview and description of models, simulations and climate diagnostics". In: *Geoscientific Model Development* 6(1), pp. 179–206. DOI: 10.5194/gmd-6-179-2013.

Lamb, D. and Verlinde J. (2011). *Physics and chemistry of clouds*. Cambridge: University Press. DOI: 10.1017/CBO9780511976377.

Lelieveld, J. et al. (2016). "Global tropospheric hydroxyl distribution, budget and reactivity". In: *Atmospheric Chemistry and Physics* 16(19), pp. 12477–12493. DOI: 10.5194/acp-2016-160.

Levy, H. (1971). "Normal atmosphere: Large radical and formaldehyde concentrations predicted". In: *Science* 173(3992), pp. 141–143. DOI: 10.1126/science.173.3992.141.

— (1973). "Tropospheric budgets for methane, carbon monoxide, and related species". In: *Journal of Geophysical Research* 78(24), pp. 5325–5332. DOI: 10.1029/JC078i024p05325.

Max-Planck-Institut für Meteorologie (n.d.). *Reducing the physical spin-up-time of the climate model land surface scheme JSBACH*. URL: https://www.mpimet.mpg.de/wissenschaft/land-im-erdsystem/master-und-bachelorarbeiten/reducing-model-spinup/?fbclid=IwAR1HKAxBNB5nYy63eEtwnqec8CKi1k2zlDwgWdw4miAoLzwY1iNHpL2pIjk. (accessed: 20.07.2020).

McNorton, J. et al. (2016). "Role of OH variability in the stalling of the global atmospheric CH4 growth rate from 1999 to 2006". In: *Atmospheric Chemistry and Physics* 16(12), pp. 7943–7956. DOI: 10.5194/acp-2015-1029.

Myhre, G. et al. (2013). "Anthropogenic and Natural Radiative Forcing." In: *Climate Change 2013: The Physical Science Basis. Contribution of Working Group I to the Fifth Assessment Report of the Intergovernmental Panel on Climate Change*. Cambridge University Press. Chap. 8, pp. 661–684.

Naik, V. et al. (2013). "Preindustrial to present-day changes in tropospheric hydroxyl radical and methane lifetime from the Atmospheric Chemistry and Climate Model Intercomparison Project (ACCMIP)". In: *Atmospheric Chemistry and Physics* 13(10), pp. 5277–5298. DOI: 10.5194/acp-13-5277-2013.

Nicely, J. M. et al. (2018). "Changes in global tropospheric OH expected as a result of climate change over the last several decades". In: *Journal of Geophysical Research: Atmospheres* 123(18), pp. 10–774. DOI: 10.1029/2018JD028388.

Nisbet, E. G. et al. (2016). "Rising atmospheric methane: 2007–2014 growth and isotopic shift". In: *Global Biogeochemical Cycles* 30(9), pp. 1356–1370. DOI: 10.1002/2016GB005406.

Nisbet, E. G. et al. (2019). "Very strong atmospheric methane growth in the 4 years 2014–2017: Implications for the Paris Agreement". In: *Global Biogeochemical Cycles* 33(3), pp. 318–342. DOI: 10.1029/2018GB006009.

Prather, M. J. (1986). "Numerical advection by conservation of second-order moments". In: *Journal of Geophysical Research: Atmospheres* 91(D6), pp. 6671–6681. DOI: 10.1029/JD091iD06p06671.

Prather, M. J. et al. (2008). "Quantifying errors in trace species transport modeling". In: *Proceedings of the National Academy of Sciences* 105(50), pp. 19617–19621. DOI: 10.1073/pnas.0806541106.

Reger, D.L., Goode S.R., and Ball D.W. (2009). *Chemistry: principles and practice*. Boston: Cengage Learning.

Rigby, M. et al. (2017). "Role of atmospheric oxidation in recent methane growth". In: *Proceedings of the National Academy of Sciences* 114(21), pp. 5373–5377. DOI: 10.1073/pnas.1616426114.

Saunois, M. et al. (2016). "The global methane budget 2000–2012". In: *Earth System Science Data* 8(2), pp. 697–751. DOI: 10.5194/essd-2016-25.

Schulzweida, U., Kornblueh L., and Quast R. (2006). "CDO user's guide". In: *Climate data operators, Version* 1(6).

The National Severe Storms Laboratory, NSSL (n.d.). *Frequently Asked Questions About Lightning*. URL: https://www.nssl.noaa.gov/education/svrwx101/lightning/faq/. (accessed: 30.07.2020).

Tiedtke, M. (1989). "A comprehensive mass flux scheme for cumulus parameterization in large-scale models". In: *Monthly Weather Review* 117(8), pp. 1779–1800. DOI: 10.1175/1520-0493(1989)117<1779:ACMFSF>2.0.CO;2.

Tronstad, M. L. (2020). Personal communication. Senior Researcher, CICERO.

Turner, A. J. et al. (2017). "Ambiguity in the causes for decadal trends in atmospheric methane and hydroxyl". In: *Proceedings of the National Academy of Sciences* 114(21), pp. 5367–5372. DOI: 10.1073/pnas.1616020114.

Voulgarakis, A. et al. (2013). "Analysis of present day and future OH and methane lifetime in the ACCMIP simulations". In: *Atmospheric Chemistry and Physics* 13(5), pp. 2563–2587. DOI: 10.5194/acpd-12-22945-2012.

Wallace, J. M. and Hobbs P. V. (2006). *Atmospheric science: an introductory survey*. Cambridge, Massachusetts: Elsevier Academic press.

Walling, C. T. (2018). "Radical". In: *Encyclopædia Britannica*. URL: https://www.britannica.com/science/radical-chemistry. accessed: 31.05.2020.

Young, P. J. et al. (2013). "Pre-industrial to end 21st century projections of tropospheric ozone from the Atmospheric Chemistry and Climate Model Intercomparison Project (ACCMIP)". In: *Atmospheric Chemistry and Physics* 13(4), pp. 2063–2090. DOI: 10.5194/acp-13-2063-2013. URL: https://acp.copernicus.org/articles/13/2063/2013/.

Appendix A

Makefile settings

Variable	Function	Chosen option
HWINDOW	Horizontal resolution (choises: HORIGINAL, HTWO, HFOUR)	**HTWO**
COLLAPSE	Collapse layer 1-3 and 4-5 into two layers	**Turned off**
OSLOCHEM	Compile with Oslo chemistry/physics	**Turned on**
TROPCHEM	Compile with Oslo tropospheric chemistry	**Turned on**
STRATCHEM	Compile with Oslo stratospheric chemistry	**Turned on**
SULPHUR	Sulphur chemistry and sulphate	**Turned on**
BCOC	Black and orgaic carbon package	**Turned off**
NITRATE	Nitrate package	**Turned on**
SEASALT	Sea salt package	**Turned on**
DUST	Mineral dust package	**Turned off**
SOA	Secondary organic aerosol package	**Turned off**
E90	e90 tracer for STE**??** flux calculations and to produce the tropopause	**Turned on**
LINOZ	Linoz O_3 for STE flux calculations	**Turned off**

Table A.1: These are the Makefile user settings chosen for all simulations in this thesis.

Appendix B

Additional Figures

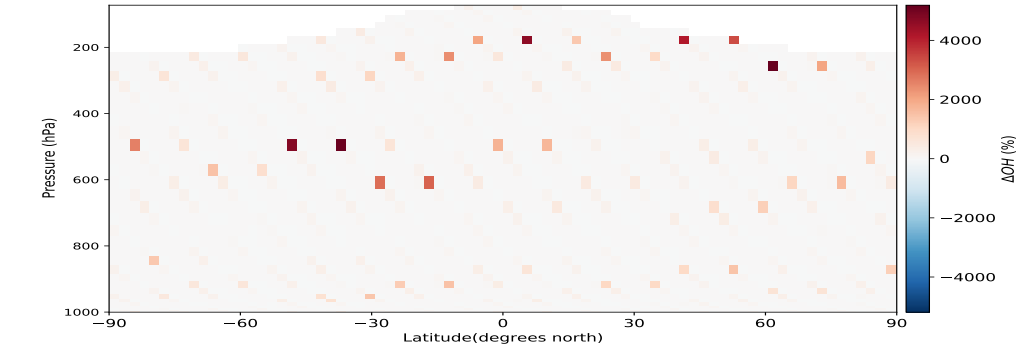

(a) ΔOH =2014n-1850n

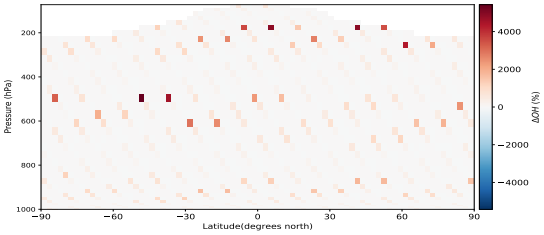

(b) ΔOH =2014rN-1850rN

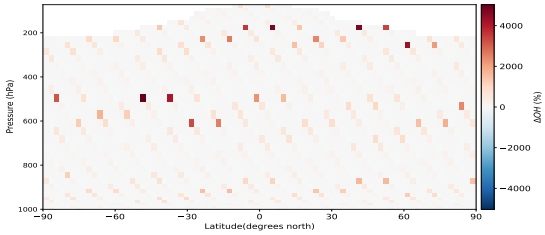

(c) ΔOH =2014rO-1850rO

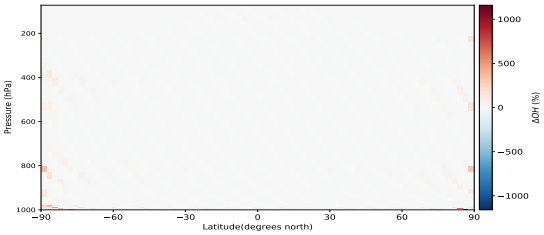

(d) ΔOH =|(2014rN-1850rN)|-|(2014n-1850n)|

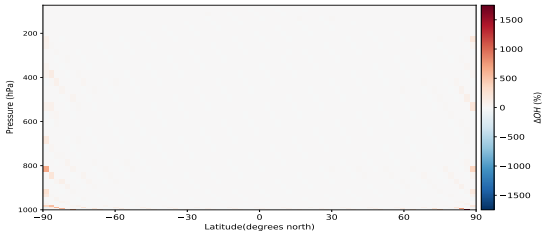

(e) ΔOH =|(2014rO-1850rO)|-|(2014n-1850n)|

Figure B.1: Vertical and latitudinal hydroxyl radical concentration distribution. The change between 1850 and 2014 for the normal scenario is shown in (a), while (b) and (c) shows the same change, respectively, for the rN and rO scenarios. The difference in change between the rN and rO scenarios and the normal is seen, respectively, in (d) and (e). Note that each part of the figure has its own colour bar, and that these differ.